# The Origin and Composition of Metasomatic Fluids and Amphiboles beneath Malaita, Solomon Islands

CLIVE R. NEAL*

*Department of Earth Sciences, The University, Leeds, LS2 9JT*

*(Received 20 March 1987; revised typescript received 9 September 1987)*

## ABSTRACT

A suite of mantle peridotite xenoliths from the Malaitan alnoite display both trace element enrichment and modal metasomatism. Pargasitic amphibole is present in both garnet- and spinel-bearing xenoliths, formed by reaction of a metasomatic fluid (represented by $H_2O$ and $Na_2O$) with the peridotite assemblage. Two pargasite-forming reactions are postulated, whereby spinel is totally consumed:

$$6MgAl_2O_4 + 8CaMgSi_2O_6 + 7Mg_2Si_2O_6 + 4H_2O + 2Na_2O = 4NaCa_2Mg_4Al_3Si_6O_{12}(OH)_2 + 6Mg_2SiO_4$$

or spinel is both a reactant (low Cr) and a product (high Cr):

$$24MgAlCrO_4 + 16CaMgSi_2O_6 + 14Mg_2Si_2O_6 + 8H_2O + 4Na_2O = 8NaCa_2Mg_4Al_3Si_6O_{12}(OH)_2 + 12MgCr_2O_4 + 12Mg_2SiO_4.$$

Seven garnet–spinel-peridotites display cryptic metasomatism as demonstrated by the LREE enrichment in clinopyroxenes. The LREE enrichment correlates positively with $^{143}Nd/^{144}Nd$ (0·512771–0·513093) which defines a mixing line between a mantle MORB source and a metasomatic fluid. Isotopic evidence (Sr and Nd) from garnet, clinopyroxene, and amphibole demonstrate this fluid has not originated in the alnoite *sensu stricto*. Calculated amphibole equilibrium liquids show a range in La/Yb and Ce/Yb ratios similar to those calculated for the augite and subcalcic diopside megacrysts. Sr and Nd isotope analyses from amphibole are within error of the augite (PHN4074) and subcalcic diopside megacrysts (CRN216, PHN4069, and PHN4085). It is concluded that fluids emanated from a *proto-alnoite* magma throughout megacryst fractionation, and the mixing line was generated during the crystallization of the subcalcic diopsides. This study demonstrates that metasomatism represented in these xenoliths is not a prerequisite for alnoite magmatism, but is a consequence of it.

## INTRODUCTION

Attempts to constrain the composition of the source for mantle-derived alkali basalt and kimberlite magmas indicate that the mantle may be enriched in incompatible elements relative to estimates of primitive mantle compositions (e.g., Kay & Gast, 1973; Sun & Hanson, 1975; Frey *et al.*, 1978; Clague & Frey, 1982). This enrichment is considered to have been facilitated by the process of *mantle metasomatism* which involves the percolation of fluids (hydrous and/or silicate) rich in incompatible elements, through the mantle. Mantle metasomatism may be expressed by the precipitation of hydrous phases, such as mica, amphibole or apatite (e.g., Menzies & Murthy, 1980*a*; Menzies & Wass, 1983), the *modal*

*Present address: Department of Geological Sciences, The University of Tennessee, Knoxville, Tennessee, 37996-1410

*metasomatism* of Harte (1983) and Menzies *et al.* (1983). Mantle metasomatism may also be expressed by the general increase of incompatible elements in the original mantle peridotite with no mineralogical modification, the *cryptic metasomatism* of Dawson (1984) and Menzies *et al.* (1985). However, in a recent discussion of terminology, Menzies & Hawkesworth (1987) have replaced this term with *trace element enrichment*.

The occurrence of amphibole in mantle derived xenoliths has been described by a number of authors (e.g., Best, 1970, 1974, 1975; Varne, 1970; Boyd, 1971; Varne & Graham, 1971; Francis, 1976, 1978; Menzies & Murthy, 1980*a*,*b*; Wilshire *et al.*, 1980; Bergmen *et al.*, 1981; Roden *et al.*, 1984). Amphibole crystallization is controlled primarily by pressure and temperature (Green, 1973; Wyllie, 1978, 1980), by migration of fluids (whether silicate or aqueous), and interaction with peridotite wallrock. Combinations of these processes have given rise to the petrographic and chemical variations in amphibole-bearing xenoliths observed by Best (1974). Isotopic studies of modal metasomatized peridotite xenoliths suggest modal metasomatism occurred $<200$ Ma prior to eruption of the host volcanic (Menzies & Murthy, 1980*a*,*b*; Stosch & Seck, 1980; Zindler & Jagoutz, 1980; Roden *et al.*, 1984). Roden *et al.* (1984) have addressed the question of whether metasomatism of mantle peridotite xenoliths, either cryptic or modal, is a prerequisite for alkali basalt generation (Kay & Gast, 1973; Boettcher *et al.*, 1979; Menzies & Murthy, 1980*a*,*b*; Wass & Rogers, 1980) or is a consequence of it (Wilshire *et al.*, 1980; Wyllie, 1980; Bergman *et al.*, 1981), concluding that at Nunivak, Alaska, metasomatism is a consequence of host volcanism.

This paper is intended to define feasible balanced chemical reactions for amphibole crystallization extending and clarifying those already postulated by Conquere (1971), Best (1974), and Francis (1976). Metasomatism, both modal and enrichment in trace elements, is identified in a suite of mantle peridotite xenoliths, consisting of 1 garnet, 9 garnet–spinel and 7 spinel lherzolites, from the Malaitan alnoite, Solomon Islands. Isotopic analyses (Sr and Nd) and rare earth element (REE) determinations have been undertaken on ultrapure mineral separates of clinopyroxene, garnet, and amphibole from these mantle periodotites to interpret the mode of origin and composition of the metasomatic fluid, and to indicate the timing of amphibole crystallization relative to the eruption age of the host alnoite (34 Ma, Davis, 1977). Such an approach can define whether mantle metasomatism recorded in these xenoliths is precursory to, or a possible consequence of, alnoite magmatism.

## PETROGRAPHY

All xenoliths studied are lherzolites that contain no fresh olivine, which is a feature of almost all mantle xenoliths from Malaita (Neal, 1985). Olivine has been altered to serpentine and chlorite, and partially replaced by carbonate. This alteration coupled with generally large grain size of the peridotites, has rendered point counting of modal proportions impossible. Table 1 represents estimated modal proportions of constituent minerals calculated by careful thin section examination. All xenoliths reported here have a coarse-equant texture, with the exception of the garnet-peridotite (PHN4034) which has a predominantly granuloblastic texture (Harte, 1977). Clinopyroxene is more abundant and generally less altered than orthopyroxene.

The spinel-lherzolites (SL) show varying degrees of amphibole development. In these seven xenoliths, amphibole occurs as a replacement of clinopyroxene and spinel. Modal per cent amphibole increases from PHN4022(SL) and CRN205(SL) (containing 2 and 5 per cent amphibole respectively) where amphibole occurs as thin ($\cong 0{\cdot}3$ mm) rinds around clinopyroxene and spinel (Fig. 1 a, b) to PHN4074(SL) (28 per cent amphibole). In PHN4028(SL) (9 per cent amphibole) amphibole forms a thicker ($\cong 0{\cdot}5$ mm) mantle around embayed spinel.

TABLE 1

*Modal mineralogy of Malaitan spinel- and garnet–spinel-lherzolites*

| | *Opx* | *Cpx* | *Spinel* | *Olivine* | *Amph.* | *Garnet* |
|---|---|---|---|---|---|---|
| PHN4022 | 4 | 20 | 4 | 70 | 2 | |
| PHN4028 | 6 | 36 | 9 | 40 | 9 | — |
| PHN4073 | 8 | 10 | 2 | 68 | 12 | — |
| PHN4074 | 3 | 3 | 2 | 64 | 28 | — |
| PHN4085 | 10 | 13 | 3 | 49 | 25 | — |
| CRN205 | 2 | 12 | 7 | 74 | 5 | — |
| CRN216 | 8 | 10 | 1 | 60 | 21 | — |
| PHN4002 | 10 | 15 | 3 | 66 | 2 | 4 |
| PHN4009 | 12 | 20 | 5 | 57 | 5 | 1 |
| PHN4013 | 12 | 13 | 3 | 56 | 6 | 10 |
| PHN4016 | 12 | 24 | 2 | 60 | — | 2 |
| PHN4034 | 5 | 9 | — | 66 | 18 | 2 |
| PHN4064 | 5 | 17 | 4 | 66 | Tr | 8 |
| PHN4067 | 5 | 28 | 3 | 58 | Tr | 6 |
| PHN4069 | 8 | 15 | 3 | 60 | 7 | 7 |
| CRN209 | 8 | 16 | 4 | 66 | 4 | 2 |
| CRN213 | 12 | 18 | 5 | 61 | Tr | 4 |

PHN4073(SL) (12 per cent amphibole) contains extremely embayed spinel and clinopyroxene (Fig. 1c). In this specimen amphibole is pervasive along the cleavage planes of clinopyroxene (Fig. 1d) which contains many exsolution lamellae. Highly embayed spinel also occurs in PHN4085(SL) (25 per cent amphibole) and CRN216(SL) (16 per cent amphibole) (Fig. 1e). This texture is similar to that seen in xenoliths from Nunivak Island, Alaska (Francis, 1976). Abundant triple junctions between phases in PHN4074(SL) (28 per cent amphibole) attest to textural equilibrium between amphibole and interstitial spinel. Clinopyroxene is present only as a few altered crystals which have attempted to equilibrate with amphibole (Fig. 1f).

The garnet–spinel-lherzolites (GSL) (PHN4002, PHN4009, PHN4013, PHN4016, PHN4016, PHN4064, PHN4067, PHN4069, CRN209, and CRN213) have pyroxene grain sizes of up to 8 mm diameter with an average of 5 mm. The garnet–spinel relationships have been described by Neal & Nixon (1986). Garnet has formed by two reactions: (1) involving clinopyroxene and spinel (PHN4013 and PHN4069); (2) involving amphibole and spinel (as in the remaining garnet–spinel-lherzolites). Amphibole is present (except PHN4016, PHN4064, PHN4067, and CRN213) and has the same textural relationships as in the spinel-lherzolites, in that it is developed around spinel (Fig. 2a) and clinopyroxene (Fig. 2b). Spinel mantled by amphibole is black and that mantled by garnet is dark brown. Garnet is fresh (except in CRN209, where it has kelyphitized margins) and appears unaffected by amphibole growth, as it is a requirement for garnet growth in some garnet–spinel-lherzolites (Neal & Nixon, 1986).

PHN4034 is an amphibole-bearing garnet-lherzolite (GL) which may be the ultimate result of the garnet-forming reaction(s) in that spinel has been totally consumed. The assemblage consists of altered olivine > amphibole > clinopyroxene > orthopyroxene > garnet (Table 1). Small garnets ($\cong$ 1 mm diameter) are set in amphibole, clinopyroxene, and orthopyroxene (1–2 mm diameter; Fig. 2c). A granuloblastic texture predominates (Harte, 1977).

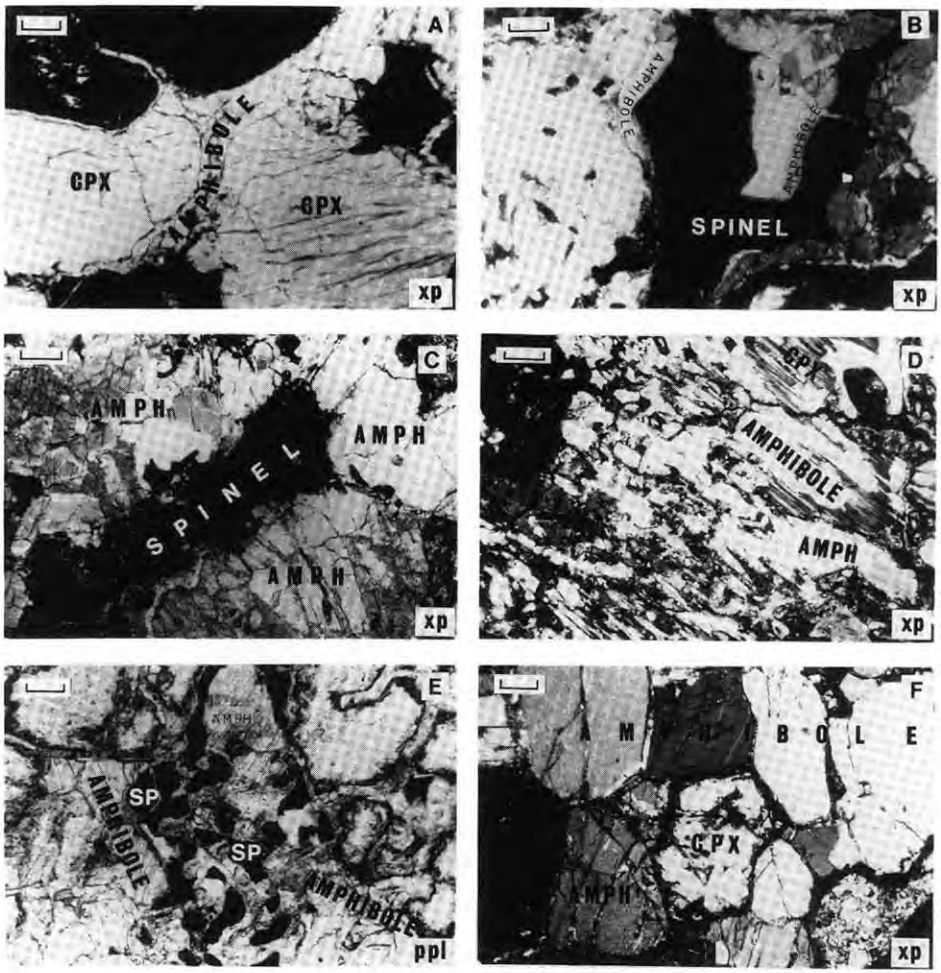


FIG. 1. Series of photomicrographs outlining the development of amphibole in spinel peridotites. (a) Development of amphibole around clinopyroxene in CRN205. Amphibole is present as a thin rind around the clinopyroxene grain. Scale bar = 0·5 mm. xp = crossed polars. (b) Development of amphibole around spinel in PHN4022. In this section amphibole is present as a thin around spinel. Scale bar = 0·25 mm. (c) More extensive development of amphibole in PHN4073. Spinel in this section is extensively embayed. Scale bar = 0·5 mm. (d) Amphibole is developed around clinopyroxene in PHN4073. Note that amphibole is pervading down the cleavage planes of clinopyroxene. Scale bar = 0·5 mm. (e) Heavily embayed spinel in PHN4085. Note the small, wormy appearance of spinel. Scale bar = 0·5 mm. ppl = plane polarized light. (f) Equilibrium texture of amphibole and clinopyroxene in PHN4074. However, note the altered nature of the clinopyroxene suggesting true equilibrium has not been attained. Scale bar = 0·5 mm.

## MAJOR ELEMENT MINERAL CHEMISTRY

### *Clinopyroxene*

Clinopyroxenes in all but one of the xenoliths studied have similar proportions of Ca : Mg : Fe (CaO = 20·4–23·6 wt. per cent; MgO = 13·8–16·6 wt. per cent; FeO = 1·7–3·0 wt. per cent: see Fig. 3 and Table 2). CRN209(GSL) is an exception in that the clinopyroxene, with elevated Mg and Fe, is subcalcic (14·8 wt. per cent CaO; 18·4 wt. per cent MgO; 3·8 wt.

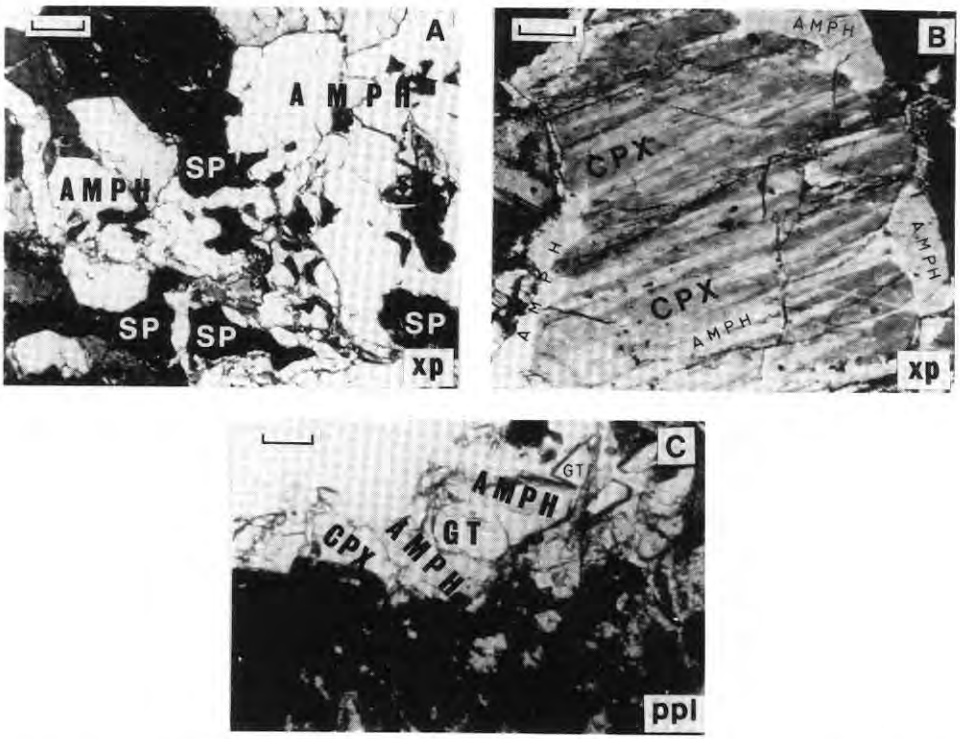


FIG. 2. Series of photomicrographs outlining the development of amphibole in the garnet-bearing peridotites. (a) Development of amphibole around spinel in PHN4069. Note the embayed nature of spinel. Scale bar = 0·5 mm. (b) Development of amphibole around clinopyroxene in PHN4013. Note how amphibole is pervading down the clinopyroxene cleavage planes. Scale bar = 0·25 mm. (c) Small garnets set in amphibole, clinopyroxene, and orthopyroxene in PHN4034. Scale bar = 0·25 mm.

per cent FeO). This may be indicative of derivation from a higher temperature regime relative to the other xenoliths (e.g., Lindsley & Andersen, 1983). CRN209(GSL) and PHN4034(GL) have higher $Cr_2O_3$ (2·3 and 1·4 wt. per cent respectively) that the rest of the xenoliths studied (0·63–0·80 wt. per cent). $Al_2O_3$, $TiO_2$, and $Na_2O$ are variable (2·4–6·5 wt. per cent, 0·10–1·08 wt. per cent and 0–2·2 wt. per cent respectively) showing no distinct preference for any of the three xenolith groups defined by petrography.

### *Orthopyroxene*

Orthopyroxenes contain similar proportions of Ca:Mg:Fe (0·38–0·60 wt. per cent CaO; 32·3–34·1 wt. per cent MgO; 5·3–6·8 wt. per cent FeO), as seen in Fig. 3 and Table 3. Exceptions to this are PHN4074(SL) (31·2 wt. per cent MgO; 9·7 wt. per cent FeO) and CRN209(GSL) (1·74 wt. per cent CaO; 31·6 wt. per cent MgO). $Al_2O_3$ contents have similar ranges for both garnet-bearing and spinel-lherzolites (1·15–5·2 wt. per cent). $Cr_2O_3$ shows little variation throughout (0·23–0·51 wt. per cent), except in CRN209(GSL) (1.10 wt. per cent).

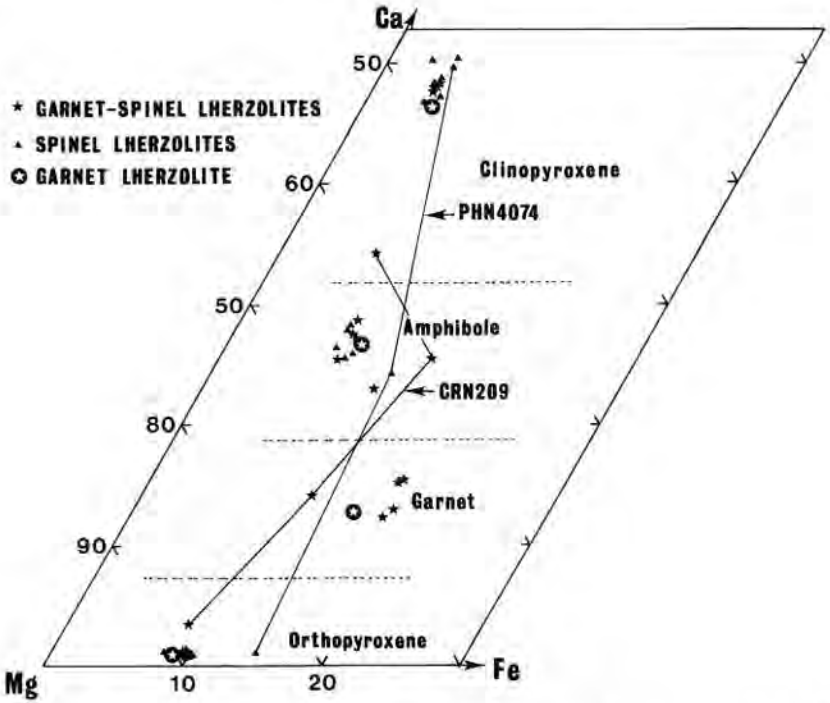


FIG. 3. Clinopyroxene, amphibole, garnet, and orthopyroxene compositions of the amphibole-bearing lherzolites represented on a Ca, Mg, Fe ternary diagram.

### *Spinel*

Spinel shows a marked variation in Cr and Al (Table 4), Cr/(Cr + Al) varying from 0·098 in CRN205(SL) to 0·694 in PHN4074(SL) and the range displayed by the spinel-lherzolites encompasses that of garnet–spinel varieties. $Fe_2O_3$ (calculated by stochiometry) shows less variation with six of the seven xenoliths falling within the range of 0·82–7·24 wt. per cent $Fe_2O_3$. Spinel in PHN4074(SL) has elevated $Fe^{3+}$ (18·5 wt. per cent $Fe_2O_3$). Mg/(Mg + $Fe^{2+}$) correlates with Cr/(Cr + Al), as in Fig. 4 (similar to that reported from Nunivak Island, Alaska, by Francis, 1976), but CRN209(GSL) plots above this general negative correlation. The range of Mg/(Mg + $Fe^{2+}$) displayed by the spinel lherzolites encompasses that of the garnet–spinel-lherzolites. $TiO_2$ is generally $<0{\cdot}60$ wt. per cent although CRN209(GSL) and PHN4074(SL) have elevated contents, 1·53 and 3·4 wt. per cent respectively.

### *Amphibole*

Amphibole is present in all seven spinel-lherzolites and in eight garnet-bearing lherzolites. Traces of amphibole between garnet and spinel have been noted in PHN4064 and PHN4067, but are not considered to be the primary result of fluid influx (Neal, 1985; Neal & Nixon, 1986) and will not be considered here.

Amphibole compositions fall into two groups according to proportions of Ca, Mg, and Fe (Fig. 3). Ten xenoliths contain amphiboles of Ca/(Ca + Mg) ranging from 0·279 to 0·311 and Mg/(Mg + Fe) from 0·873 to 0·892. Three xenoliths (PHN4074(SL), PHN4002(GSL)

and CRN209(GSL)) contain amphiboles of lower, but overlapping Ca/(Ca + Mg) (0·277, 0·261, and 0·300 respectively) and lower Mg/(Mg + Fe) ratios (0·829, 0·841, and 0·797 respectively: see Table 5). $Al_2O_3$ ranges from 10·7 to 15·9 wt. per cent; $Cr_2O_3$ and $Na_2O$ show less variation (0·17–1·74 wt. per cent and 3·35–4·85 wt. per cent respectively). Potassium (<0·10–1·41 wt. per cent $K_2O$) is detectable in all but two of the analysed amphiboles (CRN205(SL) and PHN4009(GSL)). No zonation in individual grains was noted in any specimen. These amphiboles may be generally termed pargasites after the classification of Leake (1978).

### *Garnet*

The ten garnet-bearing xenoliths contain garnets of variable Ca, Mg, and Fe contents (Fig. 3 and Table 6). Ca/(Ca + Mg) varies from 0·151 to 0·188 and Mg/(Mg + Fe) varies from 0·785 to 0·857. $Al_2O_3$ is approximately 22 wt. per cent in all except CRN213 and CRN209 (24·0 and 20·1 wt. per cent respectively). $Cr_2O_3$ varies from 0·61 to 4·90 wt. per cent. $TiO_2$ is usually present at <0·15 wt. per cent except in CRN209 where it reaches 0·56 wt. per cent. See Neal & Nixon (1986) for a full discussion of the compositional variations.

## WHOLE ROCK CHEMISTRY

The altered nature of olivine has prevented meaningful whole rock analysis of these xenoliths. However, whole rock compositions may be estimated using modal analyses and mineral data presented above. An olivine composition of $Fo_{89}$ has been used in these calculations, which was measured from a relict core in CRN211 (see Neal, 1985). Although not accurate (and, as such, compositions may not be compared with similar xenoliths from other localities), the calculated compositions (Table 7) may be compared with each other.

Elemental abundances have been plotted against modal per cent amphibole to estimate the composition of the metasomatic fluid which has infiltrated these xenoliths. Figure 5 a, b and c display the only positive correlations observed, indicating that amphibole addition contributed alkalis and $TiO_2$, as well as water, to the original anhydrous periodotite assemblage. Ca, Mg, and Fe may also have been added, but as minerals rich in these elements are present in peridotite, any correlations have been effectively masked. The calculated whole rock compositions are quite variable, which may be indicative of the inaccuracy of this method, or that the xenoliths have undergone varying degrees of partial melting (depletion in basaltic components such as Ca, Al, and Fe: e.g., O'Hara *et al.*, 1975; Nixon *et al.*, 1981) and/or metasomatic enrichment (as evidenced by varying modal per cent amphibole). For instance, CRN209(GSL) is depleted in basaltic components relative to other xenoliths, except for Fe, suggesting depletion followed by selective enrichment (see Dawson, 1984).

## ISOTOPE ANALYTICAL TECHNIQUES

Where possible, amphiboles, clinopyroxenes, and garnets were separated and meticulously handpicked under the binocular microscope. Each separate was progressively leached in an ultrasonic bath, first in 6M HCl for 1 hour, and then in a mixture of 6M HCl and 40 per cent hydrofluoric acid for 10 min to ensure no surface contamination. After each leach, the mineral separate was washed in distilled water, dried, and re-handpicked. Sub-boiled, quartz-distilled reagents were routinely used.

Sr, Nd, and the rare earth elements (REE) were separated on ion exchange columns and

TABLE 2

*Clinopyroxene compositions from Malaitan lherzolites*

| | *SL PHN4022* | *SL PHN4028* | *SL PHN4073* | *SL PHN4074* | *SL PHN4085* | *SL CRN205* | *SL CRN216* | *GSL PHN4002* |
|---|---|---|---|---|---|---|---|---|
| $SiO_2$ | 52·2 | 53·3 | 54·1 | 51·7 | 53·1 | 52·9 | 51·1 | 52·7 |
| $TiO_2$ | 0·42 | 0·10 | 0·16 | 0·53 | 0·24 | 0·46 | 1·08 | 0·54 |
| $Al_2O_3$ | 5·28 | 5·06 | 2·35 | 6·00 | 4·59 | 5·80 | 6·53 | 5·21 |
| $Cr_2O_3$ | 0·71 | 0·52 | 0·62 | 0·79 | 0·64 | 0·64 | 0·78 | 0·76 |
| FeO* | 2·55 | 1·67 | 2·61 | 2·58 | 2·96 | 2·62 | 2·51 | 2·73 |
| MnO | 0·13 | 0·09 | 0·11 | 0·12 | 0·11 | 0·09 | 0·06 | 0·05 |
| MgO | 15.1 | 15.8 | 16.6 | 14.1 | 15.3 | 15.0 | 13.8 | 14.8 |
| CaO | 22.0 | 23.6 | 22.1 | 21.5 | 21.4 | 21.3 | 21.5 | 21.0 |
| $Na_2O$ | 1·51 | — | 1·14 | 1·85 | 1·61 | 1·39 | 2·07 | 0·76 |
| Total | 99·85 | 100·14 | 99·79 | 99·17 | 99·95 | 100·20 | 99·43 | 98·55 |
| | | | *Formula moles based on 6 oxygens* | | | | | |
| Si | 1·898 | 1·919 | 1·965 | 1·892 | 1·929 | 1·907 | 1·867 | 1·915 |
| Ti | 0·012 | 0·002 | 0·004 | 0·015 | 0·007 | 0·013 | 0·030 | 0·015 |
| Al | 0·226 | 0·215 | 0·101 | 0·259 | 0·196 | 0·247 | 0·281 | 0·223 |
| Cr | 0·020 | 0·015 | 0·018 | 0·023 | 0·018 | 0·018 | 0·023 | 0·022 |
| Fe* | 0·077 | 0·051 | 0·080 | 0·079 | 0·090 | 0·079 | 0·077 | 0·083 |
| Mn | 0·044 | 0·003 | 0·003 | 0·004 | 0·004 | 0·003 | 0·003 | 0·002 |
| Mg | 0·819 | 0·848 | 0·897 | 0·769 | 0·831 | 0·808 | 0·753 | 0·804 |
| Ca | 0·856 | 0·910 | 0·861 | 0·845 | 0·824 | 0·823 | 0·842 | 0·817 |
| Na | 0·106 | — | 0·080 | 0·132 | 0·114 | 0·097 | 0·147 | 0·133 |
| Total | 4·058 | 3.963 | 4.009 | 4.018 | 4.013 | 4.074 | 4.023 | 4.016 |
| Fs | 4·4 | 2·8 | 4·4 | 4·6 | 5·2 | 4·6 | 4·6 | 4·9 |
| En | 46·7 | 46·9 | 48·8 | 44·9 | 47·6 | 47·3 | 45·0 | 47·2 |
| Wo | 48·9 | 50·3 | 46·8 | 49·3 | 47·2 | 48·1 | 50·4 | 47·9 |

* = Total Fe as FeO.

loaded on triple filaments (rhenium centre, tantalum sides) for Nd and REE analysis, and on single tantalum filaments for Sr analysis (see Neal, 1985 for a full discussion of the procedure used). External precision of Nd and Sr isotope ratios over the whole period of study was monitored by running standard samples. For Nd, 16 measurements of the La Jolla standard gave an average $^{143}Nd/^{144}Nd$ ratio of $0{\cdot}511889 \pm 20$. For Sr, 38 measurements of the NBS 987 standard gave an average $^{87}Sr/^{86}Sr$ ratio of $0{\cdot}710281 \pm 4$. A fractionation correction is applied to Nd measurements, using the $^{146}Nd/^{144}Nd$ of 0·7219. All ratios have been corrected to the age of eruption (34 Ma; Davis, 1977).

## *Isotope results*

The isotope results are discussed relative to a Bulk Earth value. Values used in this work are: $^{87}Sr/^{86}Sr = 0{\cdot}7045$; $Rb/Sr = 0{\cdot}032$; $^{143}Nd/^{144}Nd = 0{\cdot}51264$; $Sm/Nd = 0{\cdot}323$.

### *Clinopyroxene*

Clinopyroxenes from eight garnet–spinel-lherzolites and two spinel-lherzolites have $^{87}Sr/^{86}Sr$ and $^{143}Nd/^{144}Nd$ ratios (Table 8) which indicate that all the xenoliths have evolved in a system with high average Sm/Nd and low Rb/Sr ratios. Rb/Sr ratios from all analysed clinopyroxenes are all lower than the Bulk Earth value indicating the coupled nature of Rb/Sr and $^{87}Sr/^{86}Sr$ ratios. However, although spinel-lherzolite clinopyroxenes and two from the garnet–spinel-lherzolites have coupled Sm/Nd and $^{143}Nd/^{144}Nd$ (both

TABLE 2 (*continued*)

| | *GSL PHN4009* | *GSL PHN4013* | *GSL PHN4016* | *GL PHN4034* | *GSL PHN4064* | *GSL PHN4067* | *GSL PHN4069* | *GSL CRN209* | *GSL CRN213* |
|---|---|---|---|---|---|---|---|---|---|
| $SiO_2$ | 52·5 | 53·0 | 52·4 | 53·5 | 52·8 | 52·7 | 53·0 | 52·8 | 53·2 |
| $TiO_2$ | 0·53 | 0·23 | 0·70 | 0·38 | 0·53 | 0·76 | 0·26 | 0·44 | 0·52 |
| $Al_2O_3$ | 6·06 | 2·98 | 5·64 | 4·22 | 5·43 | 5·82 | 2·87 | 5·16 | 6·13 |
| $Cr_2O_3$ | 0·76 | 0·63 | 0·72 | 1·38 | 0·75 | 0·80 | 0·64 | 2·30 | 0·65 |
| FeO* | 2·61 | 2·72 | 2·43 | 2·66 | 2·76 | 2·39 | 2·68 | 3·82 | 2·33 |
| MnO | 0·11 | 0·07 | 0·11 | 0·06 | 0·06 | 0·07 | 0·05 | 0·11 | 0·09 |
| MgO | 14.7 | 16.5 | 14.8 | 15.4 | 15.0 | 14.7 | 16.4 | 18.4 | 14.9 |
| CaO | 20.9 | 23.0 | 21.2 | 20.4 | 20.6 | 20.6 | 22.6 | 14.8 | 20.9 |
| $Na_2O$ | 1·84 | 0·87 | 1·82 | 1·91 | 1·83 | 2·05 | 0·77 | 1·86 | 2·17 |
| Total | 100·01 | 100·00 | 99·82 | 99·91 | 99·74 | 99·89 | 99·27 | 99·69 | 100·42 |
| | | | | *Formula moles based on 6 oxygens* | | | | | |
| Si | 1·901 | 1·930 | 1·902 | 1·938 | 1·916 | 1·906 | 1·943 | 1·902 | 1·893 |
| Ti | 0·015 | 0·006 | 0·019 | 0·010 | 0·014 | 0·021 | 0·007 | 0·012 | 0·014 |
| Al | 0·258 | 0·128 | 0·241 | 0·180 | 0·194 | 0·248 | 0·126 | 0·219 | 0·262 |
| Cr | 0·022 | 0·018 | 0·021 | 0·039 | 0·022 | 0·023 | 0·018 | 0·065 | 0·019 |
| Fe* | 0·079 | 0·083 | 0·074 | 0·081 | 0·084 | 0·072 | 0·081 | 0·115 | 0·071 |
| Mn | 0·003 | 0·002 | 0·003 | 0·002 | 0·002 | 0·002 | 0·001 | 0·003 | 0·003 |
| Mg | 0·791 | 0·893 | 0·801 | 0·829 | 0·813 | 0·795 | 0·886 | 0·987 | 0·802 |
| Ca | 0·809 | 0·899 | 0·822 | 0·793 | 0·801 | 0·798 | 0·881 | 0·572 | 0·812 |
| Na | 0·129 | 0·061 | 0·128 | 0·134 | 0·128 | 0·144 | 0·063 | 0·130 | 0·153 |
| Total | 4.007 | 4.020 | 4·011 | 4·006 | 3·974 | 4·009 | 4·006 | 4·005 | 4·029 |
| Fs | 4·7 | 4·4 | 4·4 | 4·8 | 4·9 | 4·4 | 4·4 | 6·9 | 4·2 |
| En | 47·1 | 47·6 | 47·2 | 48·7 | 47·9 | 47·7 | 47·9 | 59·0 | 47·6 |
| Wo | 48·2 | 48·0 | 48·4 | 46·6 | 47·2 | 47·9 | 47·7 | 34·2 | 48·2 |

greater than Bulk Earth), five clinopyroxenes from garnet–spinel-lherzolites show decoupled Nd isotopes (Sm/Nd ratios < Bulk Earth, $^{143}Nd/^{144}Nd$ ratios > Bulk Earth), indicating either a recent (< 200 Ma) enrichment of the LREE, or equilibration with garnet.

*Amphibole*

Amphibole has been analysed from three spinel-lherzolites (CRN216, PHN4074 and PHN4085) and one garnet–spinel-lherzolite (PHN4069). $^{87}Sr/^{86}Sr$ and Rb/Sr ratios are coupled (both less than Bulk Earth—see Table 8). However, Sm/Nd and $^{143}Nd/^{144}Nd$ ratios are generally decoupled (Sm/Nd < Bulk Earth; $^{143}Nd/^{144}Nd$ > Bulk Earth). PHN4074 (SL) contains a Sm/Nd ratio which is approximately equal to Bulk Earth.

An important observation is that both Sr and Nd isotopic disequilibrium exists between amphibole and clinopyroxene in the two samples where both have been analysed [PHN4069 (GSL) and CRN216 (SL)].

*Garnet*

Garnet mineral separates from four garnet–spinel-lherzolites have $^{87}Sr/^{86}Sr$ and $^{143}Nd/^{144}Nd$ ratios that are lower and higher, respectively, than those of Bulk Earth (Table 8). These results are more restricted than those seen in the corresponding diopsides. The garnets show a wide range in Rb/Sr ratio (0·015–0·055), which results from the range in Sr content (4·06–12·98 p.p.m.). Sm/Nd ratios also show a wide variation (0·455–1·225), due to the extremely LREE depleted nature of PHN4064 and PHN4067 relative to PHN4013 and PHN4069. Garnet and clinopyroxene from PHN4013 and PHN4069 are in Sr and Nd isotopic equilibrium. Garnet and clinopyroxene from PHN4064 and PHN4067 are in Sr

TABLE 3

*Orthopyroxene compositions from Malaitan lherzolites*

| | *SL PHN4022* | *SL PHN4028* | *SL PHN4073* | *SL PHN4074* | *SL PHN4085* | *SL CRN205* | *SL CRN216* | *GSL PHN4002* | *GSL PHN4009* |
|---|---|---|---|---|---|---|---|---|---|
| $SiO_2$ | 54·5 | 55·3 | 54·5 | 56·2 | 54·8 | 55·4 | 56·1 | 56·3 | 55·2 |
| $TiO_2$ | 0·10 | 0·04 | 0·11 | 0·14 | 0·08 | 0·11 | 0·07 | 0·14 | 0·13 |
| $Al_2O_3$ | 4·10 | 4·45 | 4·29 | 1·15 | 5·17 | 4·69 | 3·07 | 1·90 | 3·94 |
| $Cr_2O_3$ | 0·28 | 0·28 | 0·34 | 0·23 | 0·38 | 0·33 | 0·51 | 0·32 | 0·28 |
| FeO* | 6·44 | 5·25 | 6·53 | 9·65 | 6·74 | 6·55 | 6·63 | 6·76 | 6·63 |
| MnO | 0·18 | 0·16 | 0·18 | 0·13 | 0·16 | 0·21 | 0·10 | 0·14 | 0·16 |
| MgO | 33·3 | 33·7 | 33·0 | 31·2 | 32·3 | 32·5 | 32·6 | 34·1 | 33·0 |
| CaO | 0·42 | 0·60 | 0·46 | 0·50 | 0·45 | 0·45 | 0·38 | 0·50 | 0·41 |
| Total | 99·32 | 99·78 | 99·41 | 99·20 | 100·08 | 100·24 | 99·46 | 100·16 | 99·75 |
| | | | | *Formula moles based on 6 oxygens* | | | | | |
| Si | 1·894 | 1·905 | 1·893 | 1·973 | 1·893 | 1·905 | 1·939 | 1·944 | 1·909 |
| Ti | 0·002 | 0·001 | 0·003 | 0·004 | 0·002 | 0·003 | 0·002 | 0·004 | 0·003 |
| Al | 0·167 | 0·180 | 0·176 | 0·047 | 0·210 | 0·190 | 0·125 | 0·077 | 0·161 |
| Cr | 0·008 | 0·008 | 0·008 | 0·006 | 0·010 | 0·009 | 0·014 | 0·009 | 0·008 |
| Fe* | 0·186 | 0·151 | 0·190 | 0·284 | 0·194 | 0·189 | 0·192 | 0·195 | 0·192 |
| Mn | 0·005 | 0·005 | 0·005 | 0·004 | 0·005 | 0·006 | 0·005 | 0·004 | 0·005 |
| Mg | 1·718 | 1·727 | 1·709 | 1·633 | 1·662 | 1·668 | 1·683 | 1·755 | 1·700 |
| Ca | 0·016 | 0·022 | 0·017 | 0·019 | 0·013 | 0·017 | 0·014 | 0·019 | 0·015 |
| Total | 3·996 | 3·999 | 4·001 | 3·970 | 3·989 | 3·987 | 3·974 | 4·007 | 3·993 |
| Fs | 9·7 | 7·9 | 9·9 | 14·7 | 10·4 | 10·1 | 10·2 | 9·9 | 10·1 |
| En | 89·5 | 90·9 | 89·2 | 84·3 | 88·9 | 89·0 | 89·1 | 89·1 | 89·1 |
| Wo | 0·8 | 1·2 | 8·9 | 1·0 | 0·7 | 0·9 | 0·7 | 1·0 | 0·8 |

| | *GSL PHN4013* | *GSL PHN4016* | *GL PHN4034* | *GSL PHN4064* | *GSL PHN4067* | *GSL PHN4069* | *GSL CRN209* | *GSL CRN213* |
|---|---|---|---|---|---|---|---|---|
| $SiO_2$ | 55·1 | 55·6 | 55·9 | 56·1 | 55·7 | 55·5 | 55·0 | 55·4 |
| $TiO_2$ | 0·16 | 0·19 | 0·14 | 0·17 | 0·17 | 0·13 | 0·24 | 0·09 |
| $Al_2O_3$ | 4·11 | 3·36 | 2·31 | 2·66 | 3·40 | 3·56 | 4·30 | 3·39 |
| $Cr_2O_3$ | 0·38 | 0·33 | 0·47 | 0·35 | 0·41 | 0·39 | 1·10 | 0·28 |
| FeO* | 6·69 | 6·50 | 6·02 | 6·43 | 6·32 | 6·61 | 5·55 | 6·31 |
| MnO | 0·14 | 0·14 | 0·11 | 0·19 | 0·10 | 0·10 | 0·10 | 0·15 |
| MgO | 32·9 | 33·1 | 33·5 | 33·5 | 33·3 | 33·1 | 31·6 | 33·2 |
| CaO | 0·41 | 0·44 | 0·56 | 0·46 | 0·45 | 0·40 | 1·74 | 0·42 |
| Total | 99·89 | 99·66 | 98·99 | 99·86 | 99·85 | 99·79 | 99·63 | 99·23 |
| | | | | *Formula moles based on 6 oxygens* | | | | |
| Si | 1·905 | 1·922 | 1·942 | 1·939 | 1·922 | 1·918 | 1·905 | 1·919 |
| Ti | 0·004 | 0·006 | 0·004 | 0·004 | 0·005 | 0·003 | 0·006 | 0·002 |
| Al | 0·167 | 0·137 | 0·095 | 0·108 | 0·138 | 0·157 | 0·176 | 0·139 |
| Cr | 0·010 | 0·009 | 0·013 | 0·010 | 0·011 | 0·008 | 0·030 | 0·008 |
| Fe* | 0·194 | 0·188 | 0·175 | 0·186 | 0·183 | 0·191 | 0·161 | 0·183 |
| Mn | 0·004 | 0·004 | 0·004 | 0·005 | 0·003 | 0·003 | 0·003 | 0·004 |
| Mg | 1·695 | 1·703 | 1·736 | 1·726 | 1·713 | 1·704 | 1·636 | 1·717 |
| Ca | 0·015 | 0·016 | 0·021 | 0·017 | 0·017 | 0·017 | 0·065 | 0·016 |
| Total | 3·994 | 3·985 | 3·990 | 3·995 | 3·992 | 4·001 | 4·009 | 3·987 |
| Fs | 10·2 | 9·9 | 9·1 | 9·6 | 9·6 | 10·0 | 8·6 | 9·6 |
| En | 89·0 | 89·3 | 89·8 | 89·5 | 89·5 | 89·1 | 87·9 | 89·6 |
| Wo | 0·8 | 0·8 | 1·1 | 0·9 | 0·9 | 0·9 | 3·5 | 0·8 |

*=Total Fe as FeO.

TABLE 4

*Spinel compositions from Malaitan lherzolites*

| | *SL PHN4022* | *SL PHN4028* | *SL PHN4073* | *SL PHN4074* | *SL PHN4085* | *SL CRN205* | *SL CRN216* | *GSL PHN4002* | *GSL PHN4009* |
|---|---|---|---|---|---|---|---|---|---|
| $TiO_2$ | 0·12 | 0·16 | 0·50 | 3·38 | 0·17 | 0·14 | 0·50 | 0·37 | 0·32 |
| $Al_2O_3$ | 57·7 | 55·0 | 34·7 | 10·4 | 36·7 | 57·2 | 28·0 | 45·2 | 44·5 |
| $Cr_2O_3$ | 9·87 | 11·3 | 29·3 | 35·0 | 29·6 | 9·3 | 35·7 | 21·3 | 21·1 |
| $Fe_2O_3$ | 1·95 | 3·79 | 6·09 | 18·5 | 4·62 | 2·39 | 5·73 | 2·39 | 3·79 |
| FeO | 10·4 | 9·62 | 14·9 | 24·7 | 13·7 | 10·2 | 15·1 | 2·39 | 3·79 |
| MnO | 0·16 | 0·15 | 0·31 | 0·02 | — | 0·12 | 0·36 | — | 0·05 |
| MgO | 19·5 | 19·6 | 14·7 | 7·72 | 15·7 | 20·1 | 14·2 | 17·3 | 17·7 |
| NiO | 0·41 | 0·41 | 0·21 | 0·38 | 0·03 | 0·42 | 0·24 | 0·35 | 0·33 |
| Total | 99·95 | 99·88 | 100·31 | 100·11 | 100·52 | 99·84 | 99·51 | 99·63 | 99·59 |
| | | | | *Formula moles based on 8 oxygens* | | | | | |
| Ti | 0·004 | 0·006 | 0·022 | 0·172 | 0·008 | 0·005 | 0·023 | 0·015 | 0·013 |
| Al | 3·526 | 3·402 | 2·395 | 0·822 | 2·420 | 3·522 | 1·998 | 2·938 | 2·901 |
| Cr | 0·405 | 0·468 | 1·360 | 1·864 | 1·346 | 0·383 | 1·712 | 0·929 | 0·924 |
| $Fe^{3+}$ | 0·078 | 0·144 | 0·242 | 0·948 | 0·208 | 0·090 | 0·257 | 0·118 | 0·162 |
| $Fe^{2+}$ | 0·452 | 0·419 | 0·709 | 1·397 | 0·666 | 0·408 | 0·700 | 0·565 | 0·525 |
| Mn | 0·007 | 0·007 | 0·015 | 0·002 | — | 0·006 | 0·019 | — | 0·003 |
| Mg | 1·511 | 1·536 | 1·246 | 0·775 | 1·346 | 1·568 | 1·280 | 1·423 | 1·457 |
| Ni | 0·017 | 0·018 | 0·011 | 0·020 | 0·014 | 0·018 | 0·011 | 0·012 | 0·015 |
| Total | 6·000 | 6·000 | 6·000 | 6·000 | 6·000 | 6·000 | 6·000 | 6·000 | 6·000 |
| *Cr* no. | 0·103 | 0·121 | 0·362 | 0·694 | 0·357 | 0·098 | 0·461 | 0·240 | 0·242 |
| *Mg* no. | 0·770 | 0·786 | 0·637 | 0·357 | 0·669 | 0·794 | 0·646 | 0·716 | 0·735 |

TABLE 4 (*continued*)

| | *GSL PHN4013* | *GSL PHN4016* | *GSL PHN4064* | *GSL PHN4067* | *GSL PHN4069* | *GSL CRN209* | *GSL CRN213* |
|---|---|---|---|---|---|---|---|
| $TiO_2$ | 0·37 | 0·24 | 0·60 | 0·40 | 0·41 | 1·53 | 0·20 |
| $Al_2O_3$ | 37·9 | 53·1 | 37·2 | 46·6 | 37·8 | 25·5 | 56·9 |
| $Cr_2O_3$ | 24·8 | 14·0 | 28·3 | 19·8 | 24·8 | 38·4 | 10·9 |
| $Fe_2O_3$ | 7·70 | 1·48 | 4·44 | 2·61 | 7·24 | 4·82 | 0·82 |
| FeO | 11·8 | 10·5 | 12·9 | 11·2 | 12·9 | 11·7 | 10·5 |
| MnO | 0·09 | 0·13 | 0·12 | 0·06 | 0·11 | 0·16 | 0·14 |
| MgO | 16·8 | 19·4 | 16·8 | 18·5 | 16·3 | 17·0 | 19·4 |
| NiO | 0·29 | 0·30 | — | 0·36 | 0·29 | 0·28 | 0·36 |
| Total | 99·75 | 99·15 | 100·36 | 99·53 | 99·85 | 99·39 | 99·22 |
| | | | *Formula moles based on 8 oxygens* | | | | |
| Ti | 0·016 | 0·010 | 0·026 | 0·016 | 0·018 | 0·069 | 0·008 |
| Al | 2·540 | 3·315 | 2·503 | 3·027 | 2·573 | 1·814 | 3·494 |
| Cr | 1·115 | 0·586 | 1·278 | 0·857 | 1·131 | 1·822 | 0·448 |
| $Fe^{3*}$ | 0·329 | 0·089 | 0·193 | 0·100 | 0·278 | 0·295 | 0·050 |
| $Fe^{2+}$ | 0·561 | 0·450 | 0·568 | 0·467 | 0·581 | 0·455 | 0·472 |
| Mn | 0·004 | 0·006 | 0·009 | 0·003 | 0·004 | 0·008 | 0·006 |
| Mg | 1·422 | 1·535 | 1·423 | 1·514 | 1·401 | 1·524 | 1·507 |
| Ni | 0·013 | 0·013 | — | 0·016 | 0·014 | 0·013 | 0·015 |
| Total | 6·000 | 6·000 | 6·000 | 6·000 | 6·000 | 6·000 | 6·000 |
| *Cr* no. | 0·305 | 0·150 | 0·338 | 0·221 | 0·305 | 0·501 | 0·114 |
| *Mg* no. | 0·717 | 0·773 | 0·715 | 0·714 | 0·707 | 0·770 | 0·761 |

*=Total Fe as FeO.

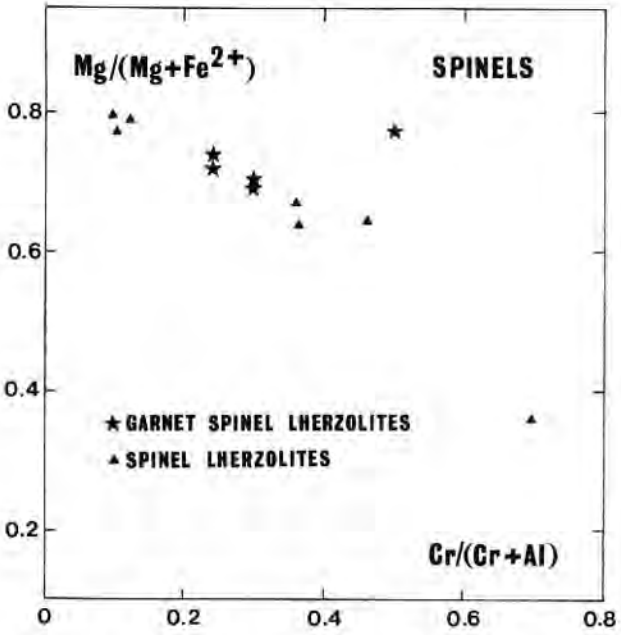


FIG. 4. $Mg/(Mg+Fe^{2+})$ v $Cr/(Cr+Al)$ for spinel compositions.

isotopic disequilibrium, with garnet containing more radiogenic $^{87}Sr/^{86}Sr$ ratios. However, Nd results are less clear: clinopyroxene and garnet from PHN4064 are in equilibrium, but those in PHN4067 appear to be in disequilibrium, with the garnet containing less radiogenic $^{143}Nd/^{144}Nd$ ratios than clinopyroxene.

## RARE EARTH ELEMENTS (REE)

The terms 'depleted' and 'enriched' are used to describe REE patterns relative to a flat, chondrite-normalized bulk earth pattern.

### *Clinopyroxene*

Clinopyroxene REE profiles range from relatively LREE enriched (PHN4013 (GSL) and PHN4069 (GSL)) to relatively LREE depleted (CRN213 (GSL)). A spectrum of REE patterns falls between these two extremes. CRN213 (GSL), CRN216 (SL), CRN205 (SL), PHN4009 (GSL), and PHN4016 (GSL) all contain LREE depleted clinopyroxenes (Fig. 6a and Table 9), with maximum abundances in the middle and heavy REE (Gd–Er). A peculiar feature of these LREE depleted samples is the inflection at La, which is exemplified by CRN205 (SL), where not only La, but Ce is enriched relative to the general LREE depleted profile. CRN209 (GSL), PHN4064 (GSL), PHN4067 (GSL), PHN4013 (GSL), and PHN4069 (GSL) all display LREE enrichment. PHN4013 and PHN4069 contain similar profiles with La/Yb ratios 53·1 and 60·3 respectively, but both have La/Ce ratios < chondrites. PHN4064 has a maximum at La, with decreasing relative abundances to Lu (La/Yb = 11·2). CRN209 and PHN4067 have similar convex-upward profiles with a maximum at

TABLE 5

*Garnet compositions from Malaitan garnet-bearing lherzolites*

| | *PHN4002* | *PHN4009* | *PHN4013* | *PHN4016* | *PHN4034* | *PHN4064* | *PHN4067* | *PHN4069* | *CRN209* | *CRN213* |
|---|---|---|---|---|---|---|---|---|---|---|
| $SiO_2$ | 41·8 | 41·9 | 41·7 | 42·2 | 42·3 | 42·1 | 42·1 | 41·7 | 41·7 | 41·6 |
| $TiO_2$ | 0·09 | 0·07 | 0·08 | 0·10 | 0·11 | 0·01 | 0·15 | 0·08 | 0·56 | 0·08 |
| $Al_2O_3$ | 22·9 | 23·0 | 22·6 | 23·0 | 22·2 | 22·9 | 22·8 | 22·3 | 20·1 | 24·0 |
| $Cr_2O_3$ | 1·01 | 0·61 | 1·32 | 0·77 | 1·78 | 0·90 | 0·84 | 1·32 | 4·90 | 0·68 |
| FeO* | 9·36 | 9·12 | 8·97 | 9·13 | 8·03 | 8·82 | 8·92 | 8·99 | 6·23 | 8·78 |
| MnO | 0·41 | 0·53 | 0·47 | 0·52 | 0·37 | 0·46 | 0·43 | 0·49 | 0·24 | 0·47 |
| MgO | 19·2 | 19·6 | 18·6 | 19·2 | 20·1 | 19·9 | 19·7 | 18·8 | 20·9 | 19·5 |
| CaO | 5·02 | 4·84 | 6·00 | 5·15 | 5·14 | 4·93 | 4·95 | 5·89 | 5·54 | 4·79 |
| Total | 99·79 | 99·67 | 99·74 | 100·07 | 100·04 | 100·02 | 99·89 | 99·77 | 100·17 | 99·90 |
| | | | | | *Formula moles based on 12 oxygens* | | | | | |
| Si | 2·985 | 2·991 | 2·989 | 3·004 | 3·007 | 2·997 | 3·001 | 3·004 | 2·976 | 2·955 |
| Ti | 0·005 | 0·004 | 0·005 | 0·005 | 0·006 | 0·005 | 0·008 | 0·005 | 0·030 | 0·005 |
| Al | 1·929 | 1·935 | 1·913 | 1·935 | 1·860 | 1·919 | 1·920 | 1·884 | 1·690 | 2·016 |
| Cr | 0·057 | 0·034 | 0·076 | 0·045 | 0·100 | 0·050 | 0·047 | 0·075 | 0·277 | 0·038 |
| Fe* | 0·560 | 0·547 | 0·538 | 0·529 | 0·477 | 0·525 | 0·532 | 0·539 | 0·372 | 0·522 |
| Mn | 0·025 | 0·032 | 0·029 | 0·033 | 0·023 | 0·028 | 0·026 | 0·030 | 0·014 | 0·028 |
| Mg | 2·050 | 2·094 | 1·992 | 2·035 | 2·131 | 2·109 | 2·092 | 2·010 | 2·223 | 2·060 |
| Ca | 0·390 | 0·371 | 0·461 | 0·393 | 0·391 | 0·376 | 0·378 | 0·453 | 0·424 | 0·366 |
| Total | 8·001 | 8·008 | 8·003 | 7·979 | 7·995 | 8·009 | 8·004 | 8·000 | 8·006 | 7·990 |
| *Cr*-no. | 0·029 | 0·017 | 0·038 | 0·020 | 0·051 | 0·025 | 0·024 | 0·038 | 0·141 | 0·019 |
| *Mg*-no. | 0·785 | 0·793 | 0·787 | 0·794 | 0·817 | 0·801 | 0·797 | 0·789 | 0·857 | 0·798 |
| *Ca*-no. | 0·160 | 0·151 | 0·188 | 0·162 | 0·155 | 0·151 | 0·153 | 0·184 | 0·160 | 0·151 |

* = Total Fe as FeO.

TABLE 6

*Amphibole compositions from Malaitan lherzolites*

| | *SL PHN4022* | *SL PHN4028* | *SL PHN4073* | *SL PHN4074* | *SL PHN4085* | *SL CRN205* | *SL CRN216* |
|---|---|---|---|---|---|---|---|
| $SiO_2$ | 43·2 | 44·0 | 43·8 | 45·4 | 44·0 | 44·1 | 45·3 |
| $TiO_2$ | 1·08 | 1·34 | 0·91 | 1·33 | 0·87 | 0·92 | 0·73 |
| $Al_2O_3$ | 15·9 | 14·7 | 14·0 | 10·7 | 14·3 | 15·3 | 13·0 |
| $Cr_2O_3$ | 0·81 | 1·05 | 1·62 | 1·13 | 1·67 | 0·84 | 1·74 |
| FeO* | 3·98 | 4·41 | 4·62 | 6·48 | 4·38 | 3·93 | 3·94 |
| MnO | 0·03 | 0·06 | 0·09 | 0·07 | 0·06 | 0·06 | 0·08 |
| MgO | 17·6 | 17·7 | 17·7 | 17·7 | 17·8 | 17·8 | 18·3 |
| CaO | 11·0 | 10·5 | 9·83 | 9·43 | 10·1 | 10·8 | 10·2 |
| $Na_2O$ | 4·07 | 3·36 | 4·49 | 4·81 | 4·09 | 3·76 | 3·35 |
| $K_2O$ | 0·02 | 0·56 | 0·64 | 0·76 | 0·51 | — | 0·70 |
| Total | 97·69 | 97·68 | 97·70 | 97·81 | 97·78 | 97·51 | 97·34 |
| | | | *Formula moles based on 23 oxygens* | | | | |
| Si | 6·135 | 6·237 | 6·243 | 6·514 | 6·243 | 6·224 | 6·246 |
| Ti | 0·115 | 0·143 | 0·097 | 0·143 | 0·065 | 0·098 | 0·078 |
| Al | 2·609 | 2·462 | 2·352 | 1·810 | 2·391 | 2·552 | 2·179 |
| Cr | 0·090 | 0·118 | 0·183 | 0·128 | 0·188 | 0·094 | 0·195 |
| Fe* | 0·472 | 0·524 | 0·551 | 0·778 | 0·520 | 0·464 | 0·467 |
| Mn | 0·004 | 0·007 | 0·011 | 0·009 | 0·007 | 0·007 | 0·010 |
| Mg | 3·753 | 3·732 | 3·771 | 3·782 | 3·768 | 3·753 | 3·873 |
| Ca | 1·667 | 1·591 | 1·500 | 1·449 | 1·468 | 1·634 | 1·546 |
| Na | 1·122 | 0·925 | 1·240 | 1·339 | 1·126 | 1·031 | 0·921 |
| K | 0·003 | 0·102 | 0·116 | 0·139 | 0·093 | — | 0·126 |
| Total | 15·970 | 15·841 | 16·064 | 16·091 | 15·869 | 15·857 | 15·821 |
| *Mg*-no. | 0·888 | 0·877 | 0·873 | 0·829 | 0·879 | 0·890 | 0·892 |
| *Ca*-no. | 0·308 | 0·299 | 0·285 | 0·277 | 0·280 | 0·303 | 0·285 |

Nd (La/Yb = 6·1 and 5·4 respectively). All LREE enriched samples have similar HREE concentrations (0·6–1·8 × chondrite), but widely varying LREE abundances (9·9–94 × chondrite).

### *Amphibole*

Four xenoliths have had amphibole analysed for the REE (Fig. 6b and Table 9). All amphiboles are LREE enriched. CRN216 (SL) and PHN4085 (SL) amphiboles have similar REE profiles (La/Yb = 5·8 and 5·0 respectively), with a maximum at Nd. Amphibole from PHN4074 (SL) has a REE pattern with a maximum at Sm and a La/Yb ratio of 3·62. Amphibole from PHN4069 (GSL) has a LREE enriched profile which is a mirror image of the co-existing clinopyroxene (La/Yb = 67·6) with a maximum at Ce, although it is less enriched overall. This REE pattern is markedly different from those of the other three analysed amphiboles.

### *Garnet*

Garnet REE abundances have been measured from five garnet–spinel-lherzolites (Fig. 6c and Table 9). All are LREE depleted, but two groups are distinguished on the basis of LREE abundances. PHN4013 and PHN4069 have $La_N$ values of $\cong 3$, whereas PHN4064,

TABLE 6 (*continued*)

| | *GSL PHN4002* | *GSL PHN4009* | *GSL PHN4013* | *GL PHN4034* | *GSL PHN4069* | *GSL CRN209* |
|---|---|---|---|---|---|---|
| $SiO_2$ | 43·7 | 45·8 | 44·2 | 44·1 | 44·0 | 42·2 |
| $TiO_2$ | 0·30 | 0·95 | 0·79 | 2·02 | 0·94 | 3·09 |
| $Al_2O_3$ | 15·3 | 12·1 | 14·5 | 13·4 | 13·9 | 14·2 |
| $Cr_2O_3$ | 0·91 | 0·61 | 1·09 | 1·56 | 1·17 | 0·70 |
| FeO* | 6·08 | 9·12 | 4·33 | 4·50 | 4·30 | 7·25 |
| MnO | 0·18 | 0·53 | 0·08 | — | 0·07 | 0·16 |
| MgO | 18·1 | 19·6 | 17·8 | 17·3 | 18·1 | 16·0 |
| CaO | 8·87 | 8·84 | 10·6 | 10·1 | 11·4 | 9·56 |
| $Na_2O$ | 4·06 | 0·17 | 3·75 | 3·40 | 3·47 | 3·53 |
| $K_2O$ | 0·15 | — | 0·32 | 1·41 | 0·06 | 1·19 |
| Total | 97·65 | 97·72 | 97·46 | 97·79 | 97·41 | 97·88 |
| | | | *Formula moles based on 23 oxygens* | | | |
| Si | 6·213 | 6·472 | 6·274 | 6·273 | 6·259 | 6·091 |
| Ti | 0·032 | 0·101 | 0·084 | 0·216 | 0·101 | 0·335 |
| Al | 2·570 | 2·016 | 2·424 | 2·256 | 2·334 | 2·406 |
| Cr | 0·102 | 0·084 | 0·122 | 0·175 | 0·131 | 0·080 |
| Fe* | 0·724 | 0·525 | 0·514 | 0·536 | 0·511 | 0·875 |
| Mn | 0·022 | 0·011 | 0·010 | | 0·008 | 0·019 |
| Mg | 3·823 | 3·978 | 3·772 | 3·680 | 3·833 | 3·441 |
| Ca | 1·351 | 1·536 | 1·615 | 1·544 | 1·734 | 1·478 |
| Na | 1·119 | 1·155 | 1·031 | 0·938 | 0·954 | 0·988 |
| K | 0·028 | 0·121 | 0·057 | 0·256 | 0·011 | 0·219 |
| Total | 15·984 | 15·999 | 15·903 | 15·874 | 15·876 | 15·932 |
| *Mg*-no. | 0·841 | 0·883 | 0·880 | 0·873 | 0·882 | 0·797 |
| *Ca*-no. | 0·261 | 0·279 | 0·300 | 0·296 | 0·311 | 0·300 |

* = Total Fe as FeO.

PHN4067 and CRN213 have $La_N$ values of <0·4. These two groups cannot be distinguished on the basis of HREE, which range from $Lu_N$ 8–34. PHN4013 has similar LREE abundances to PHN4069, but contains less HREE (La/Yb = 0·345 and 0·154 respectively). CRN213, PHN4064, and PHN4067 have similar REE profiles (La/Yb = 0·012–0·033) with a maximum at Lu.

### *Estimated whole rock REE profiles*

The whole rock REE patterns may be estimated by consideration of REE in the constituent minerals and modal abundances. Figure 7 demonstrates whole rock profiles in the garnet–spinel-lherzolites where garnet and clinopyroxene (±amphibole) have been analysed. Also included on this plot is the reconstructed whole rock REE pattern from CRN216 (SL) based on clinopyroxene and amphibole abundances. In other spinel-lherzolites, REE in clinopyroxene is taken as representative of the whole rock, except in PHN4074 where clinopyroxene is rare and amphibole is the main REE carrier.

The reconstructed whole rock REE profiles for CRN216 (SL), PHN4013 (GSL), PHN4064 (GSL), and PHN4069 (GSL) show LREE enrichment (Sm/Nd < Bulk Earth). The $^{143}Nd/^{144}Nd$ ratios for clinopyroxene, garnet, and where possible, amphibole, are all greater than Bulk Earth. Note that in PHN4013 (GSL) amphibole (6 modal per cent) has not been analysed, and it is likely that the whole rock would be elevated in LREE from the pattern calculated from just garnet and clinopyroxene. Therefore, *the decoupling of the Nd isotopic ratios seen in the mineral separates is not a function of mineral equilibration with*

TABLE 7

*Calculated whole rock compositions*

| | *SL PHN4022* | *SL PHN4028* | *SL PHN4073* | *SL PHN4074* | *SL PHN4085* | *SL CRN205* | *SL CRN216* | *GSL PHN4002* |
|---|---|---|---|---|---|---|---|---|
| $SiO_2$ | 42·3 | 42·8 | 42·9 | 42·2 | 44·0 | 42·2 | 44·0 | 42·7 |
| $TiO_2$ | 0·12 | 0·12 | 0·14 | 0·46 | 0·26 | 0·15 | 0·27 | 0·12 |
| $Al_2O_3$ | 4·10 | 7·92 | 3·17 | 3·63 | 5·92 | 6·40 | 4·11 | 3·55 |
| $Cr_2O_3$ | 0·57 | 1·27 | 0·87 | 1·05 | 1·38 | 0·81 | 0·84 | 1·05 |
| FeO* | 7·89 | 6·53 | 8·16 | 9·07 | 7·32 | 8·27 | 7·47 | 8·95 |
| MnO | 0·04 | 0·06 | 0·04 | 0·03 | 0·05 | 0·02 | 0·04 | 0·11 |
| MgO | 39·4 | 31·8 | 39·8 | 37·6 | 34·0 | 39·5 | 37·2 | 39·2 |
| CaO | 4·64 | 9·05 | 3·43 | 3·30 | 5·34 | 3·53 | 4·33 | 3·58 |
| $Na_2O$ | 0·41 | 0·17 | 0·65 | 1·43 | 1·23 | 0·51 | 0·95 | 0·20 |
| $K_2O$ | 0·01 | 0·04 | 0·08 | 0·21 | 0·13 | 0·05 | 0·15 | 0·01 |
| NiO | 0·24 | 0·17 | 0·21 | 0·25 | 0·15 | 0·24 | 0·18 | 0·26 |
| Total | 99·72 | 99·84 | 99·42 | 99·23 | 99·78 | 99·58 | 99·24 | 99·73 |

| | *GSL PHN4009* | *GSL PHN4013* | *GSL PHN4016* | *GL PHN4034* | *GSL PHN4064* | *GSL PHN4067* | *GSL PHN4069* | *GSL CRN209* | *GSL CRN213* |
|---|---|---|---|---|---|---|---|---|---|
| $SiO_2$ | 42·7 | 42·9 | 44·6 | 42·4 | 41·7 | 43·4 | 42·5 | 41·8 | 42·2 |
| $TiO_2$ | 0·19 | 0·15 | 0·20 | 0·40 | 0·12 | 0·24 | 0·14 | 0·19 | 0·12 |
| $Al_2O_3$ | 4·93 | 4·99 | 3·48 | 3·52 | 4·59 | 4·76 | 4·51 | 2·95 | 5·11 |
| $Cr_2O_3$ | 1·32 | 1·09 | 0·51 | 0·45 | 1·35 | 0·89 | 1·12 | 2·14 | 0·94 |
| FeO* | 8·37 | 8·58 | 8·19 | 8·56 | 9·09 | 8·00 | 8·76 | 8·76 | 8·54 |
| MnO | 0·12 | 0·13 | 0·12 | 0·09 | 0·13 | 0·11 | 0·12 | 0·11 | 0·24 |
| MgO | 36·5 | 36·5 | 37·8 | 38·9 | 38·4 | 35·6 | 37·2 | 39·9 | 37·8 |
| CaO | 4·78 | 4·47 | 5·23 | 3·78 | 3·92 | 6·08 | 4·64 | 2·17 | 4·01 |
| $Na_2O$ | 0·61 | 0·49 | 0·48 | 0·78 | 0·31 | 0·58 | 0·38 | 0·33 | 0·40 |
| $K_2O$ | 0·03 | 0·03 | — | 0·25 | — | — | 0·01 | 0·01 | — |
| NiO | 0·24 | 0·23 | 0·24 | 0·28 | 0·26 | 0·20 | 0·24 | 0·27 | 0·25 |
| Total | 99·79 | 99·56 | 100·85 | 99·41 | 99·87 | 99·86 | 99·62 | 99·54 | 99·67 |

*secondary garnet*. The garnet–spinel-lherzolite CRN213 has a LREE depleted whole rock profile, consistent with $^{143}Nd/^{144}Nd$ ratios greater than Bulk Earth in the mineral separates. However, PHN4067 (GSL) has a flat to slightly convex upward whole rock REE profile, but $^{143}Nd/^{144}Nd$ ratios greater than Bulk Earth. It is probable that this xenolith has also experienced some degree of LREE enrichment.

## DISCUSSION

The petrographic study (see Figs. 1 and 2) demonstrates that amphibole is growing at the expense of clinopyroxene and spinel. These textural relationships have been noted in mantle derived xenoliths from various areas by other authors (e.g., Massif Central, France: Conquere, 1971; the Grand Canyon: Best, 1974) and prompted the proposal of an amphibole-forming reaction involving clinopyroxene and spinel.

Using the unpublished computer programme of R. Powell (RE PASCAL), the feasible amphibole-forming reactions may be determined. This programme computes reactants and products based on their constituent oxides. RE PASCAL indicates that clinopyroxene,

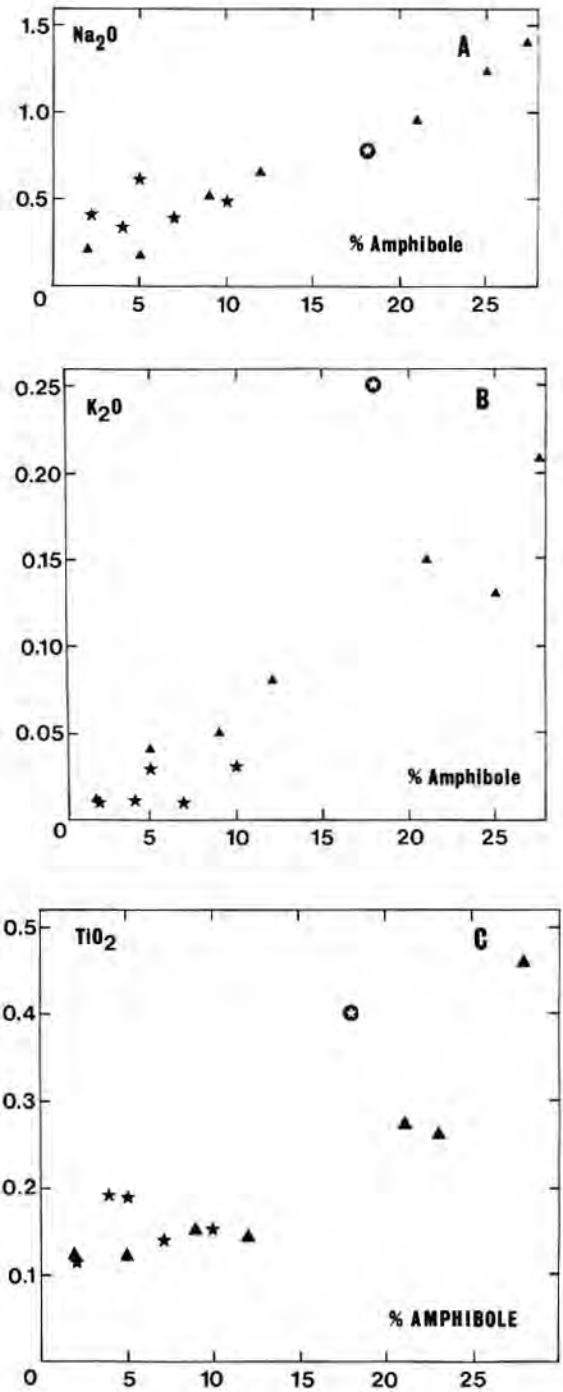


FIG. 5. Calculated whole rock compositions versus modal percent amphibole to estimate contributions to the peridotite assemblage from the metasomatic fluid: (a) whole rock $Na_2O$ vs. modal percent amphibole; (b) whole rock $K_2O$ vs. modal percent amphibole; (c) whole rock $TiO_2$ vs. modal percent amphibole. Symbols as in Fig. 3.

TABLE 8

*Rb–Sr and Sm–Nd isotope results from lherzolite mineral separates and host alnoite*

| | *Rb(p.p.m.)* | *Sr(p.p.m.)* | *Rb/Sr* | $^{87}Sr/^{86}Sr \pm 2Sd$ | *εSr* | *Sm(p.p.m.)* | *Nd(p.p.m.)* | *Sm/Nd* | $^{143}Nd/^{144}Nd \pm Sd$ | *εNd* |
|---|---|---|---|---|---|---|---|---|---|---|
| CRN205(SL) | 0·13 | 29·7 | 0·0044 | 0·702451 ± 60 | −29·1 | 1·25 | 2·40 | 0·5208 | 0·512951 ± 40 | +6·1 |
| CRN216(SL) | 0·10 | 47·7 | 0·0021 | 0·702962 ± 16 | −21·8 | 2·08 | 4·71 | 0·4416 | 0·513007 ± 28 | +7·2 |
| PHN4009(GSL) | 0·22 | 39·9 | 0·0056 | 0·703631 ± 12 | −12·3 | 1·99 | 5·28 | 0·3769 | 0·512929 ± 18 | +5·6 |
| PHN4013(GSL) | 0·32 | 272·3 | 0·0012 | 0·703931 ± 20 | −8·1 | 2·49 | 22·0 | 0·1130 | 0·512780 ± 30 | +2·7 |
| PHN4016(GSL) | 0·12 | 33·0 | 0·0037 | 0·702923 ± 12 | −22·4 | 1·26 | 2·91 | 0·4239 | 0·513041 ± 16 | +7·8 |
| PHN4064(GSL) | 0·11 | 66·2 | 0·0017 | 0·703061 ± 8 | −20·4 | 2·13 | 8·51 | 0·2491 | 0·512867 ± 20 | +4·4 |
| PHN4067(GSL) | 0·24 | 54·3 | 0·0045 | 0·702637 ± 40 | −26·4 | 1·98 | 6·17 | 0·3209 | 0·512898 ± 40 | +5·0 |
| PHN4069(GSL) | 0·48 | 400·7 | 0·0012 | 0·704047 ± 6 | −6·4 | 8·96 | 74·3 | 0·1205 | 0·512771 ± 10 | +2·6 |
| CRN209(GSL) | 0·53 | 83·2 | 0·0064 | 0·703276 ± 14 | −17·4 | 1·36 | 4·30 | 0·3163 | 0·512804 ± 14 | +3·2 |
| CRN213(GSL) | 0·13 | 20·0 | 0·0065 | 0·703295 ± 30 | −17·1 | 1·28 | 2·51 | 0·5100 | 0·513093 ± 25 | +8·8 |
| | | | | *Amphibole* | | | | | | |
| PHN4069(GSL) | 2·91 | 861·9 | 0·0034 | 0·703920 ± 40 | −8·2 | 2·71 | 23·1 | 0·1172 | 0·512842 ± 30 | +3·9 |
| PHN4074(SL) | 1·85 | 272·0 | 0·0068 | 0·703327 ± 40 | −16·7 | 4·27 | 12·7 | 0·3362 | 0·512702 ± 30 | +1·2 |
| PHN4085(SL) | 3·03 | 296·0 | 0·0102 | 0·704066 ± 12 | −6·2 | 6·84 | 25·1 | 0·2727 | 0·512791 ± 17 | +3·0 |
| CRN216(SL) | 3·24 | 362·7 | 0·0089 | 0·704053 ± 10 | −6·3 | 7·73 | 28·8 | 0·2682 | 0·512792 ± 24 | +3·1 |
| | | | | *Garnet* | | | | | | |
| PHN4013(GSL) | 0·18 | 13·0 | 0·0146 | 0·703997 ± 200 | −7·1 | 1·36 | 2·99 | 0·4669 | 0·512778 ± 30 | +1·7 |
| PHN4064(GSL) | 0·25 | 8·2 | 0·0311 | 0·704278 ± 17 | −3·2 | 0·30 | 0·39 | 0·6917 | 0·512821 ± 30 | +3·5 |
| PHN4067(GSL) | 0·22 | 4·1 | 0·0547 | 0·704305 ± 80 | −2·8 | 0·49 | 0·40 | 1·225 | 0·512776 ± 40 | +2·7 |
| PHN4069(GSL) | 0·24 | 6·8 | 0·0350 | 0·704016 ± 10 | −6·9 | 1·36 | 2·99 | 0·4548 | 0·512774 ± 19 | +2·6 |
| | | | | *Alnoite* | | | | | | |
| CRN233 | 66 | 1209 | 0·0546 | 0·704568 ± 20 | +1·0 | 15·3 | 79·7 | 0·1918 | 0·512811 ± 14 | +5·8 |
| CRN235 | 40 | 1473 | 0·0272 | 0·704645 ± 18 | +2·1 | 15·2 | 79·2 | 0·1914 | 0·512852 ± 14 | +4·1 |
| CRN237 | 66 | 928 | 0·0711 | 0·704372 ± 8 | −1·8 | 15·5 | 80·7 | 0·1917 | 0·512836 ± 13 | +3·8 |
| CRN242 | 57 | 1562 | 0·0364 | 0·704207 ± 12 | −4·2 | 16·3 | 81·2 | 0·2002 | 0·512764 ± 17 | +2·4 |

spinel, and fluid are insufficient to form the pargasitic amphibole present in the Malaitan peridotites.

Francis (1976) proposed the reaction:

$$\text{Fluid} + \text{Orthopyroxene} + \text{Clinopyroxene} + \text{Spinel} = \text{Chromite} + \text{Amphibole}$$

whereby orthopyroxene is also a reactant, and spinel is both a reactant (low Cr/(Cr + Al)) and a product (high Cr/(Cr + Al)). Two reactions are postulated from the present study and both involve a fluid phase, spinel, clinopyroxene, and orthopyroxene to form amphibole (pargasite). For simplicity, end-member compositions have been used (see Deer *et al.*, 1978) and the fluid is represented by $Na_2O$ and $H_2O$. The first reaction assumes all the spinel is consumed:

$$\underset{\text{Spinel}}{6MgAl_2O_4} + \underset{\text{CPx}}{8CaMgSi_2O_6} + \underset{\text{OPx}}{7Mg_2Si_2O_6} + \underset{\text{Fluid}}{4H_2O + 2Na_2O}$$

$$= \underset{\text{Pargasite}}{4NaCa_2Mg_4Al_3Si_6O_{12}(OH)_2} + \underset{\text{Olivine}}{6Mg_2SiO_4}$$

The second is a modification of the reaction proposed by Francis (1976) whereby spinel is

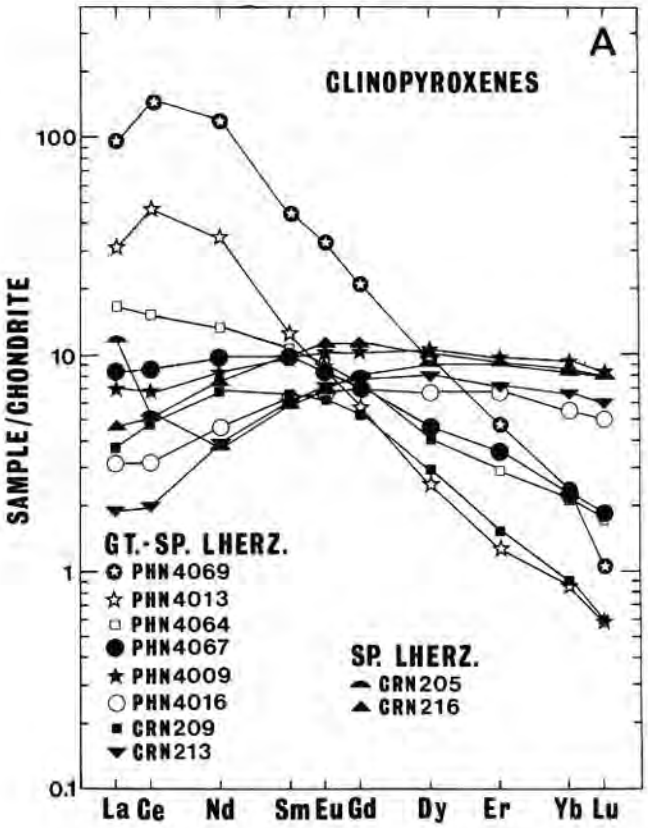


Fig. 6 A.

not totally consumed, but because of amphibole growth, has become enriched in $Cr_2O_3$:

$$24MgAlCrO_4 + 16CaMgSi_2O_6 + 14Mg_2Si_2O_6 + 8H_2O + 4Na_2O$$
Spinel CPx OPx Fluid

$$= 8NaCa_2Mg_4Al_3Si_6O_{12}(OH)_2 + 12MgCr_2O_4 + 12Mg_2SiO_4$$
Pargasite Chromite Olivine

Both reactions require the production of olivine. However, because of the altered nature of olivine in these peridotites, petrography cannot substantiate this conjecture, but spinels mantled by amphibole have an increased Cr/(Cr + Al) ratio relative to spinels unaffected by amphibole growth. The $Fe^{3+}$ content of spinel also increases in response to amphibole crystallization indicating that Cr and $Fe^{3+}$ are partitioned into the shrinking spinel phase.

It is evident that amphibole composition is dependent not only on the composition of the metasomatic fluid, but also upon that of the peridotite with which it interacts. Low $Al_2O_3$ in amphibole of PHN4074 (SL) and high $TiO_2$ in the amphibole of CRN209 (GSL) are both reflections of the spinel compositions of these xenoliths. However, the lack of chemical zoning in any of the lherzolite minerals is surprising, considering the reaction textures

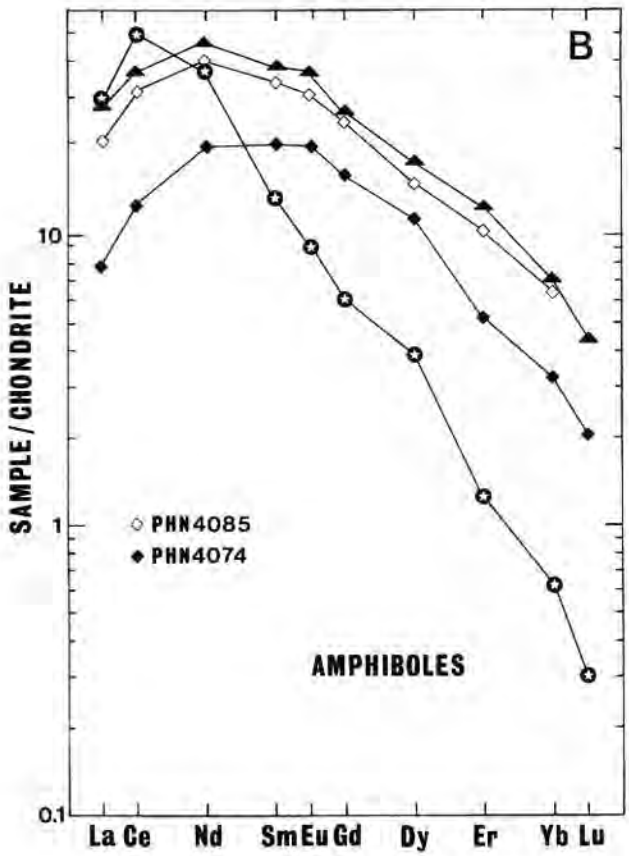


Fig. 6 B.

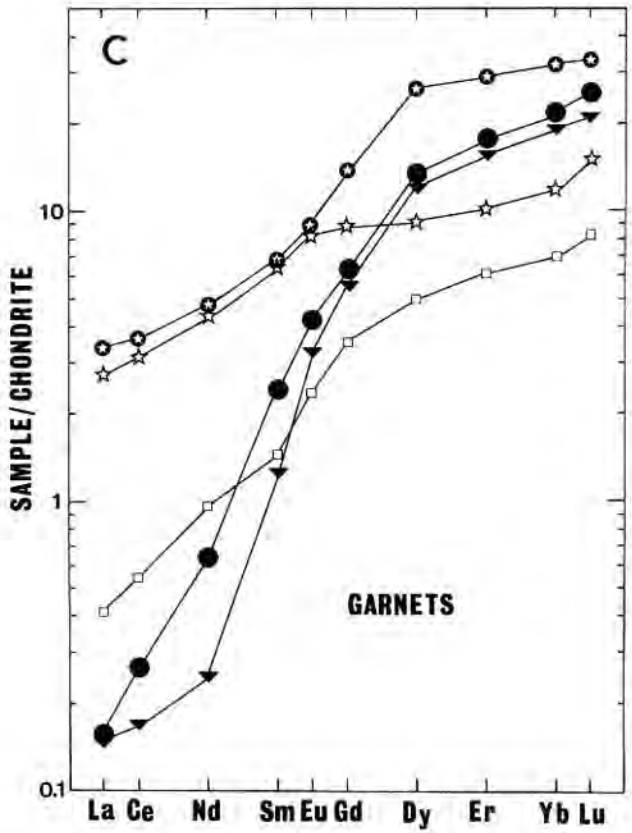


FIG. 6. Chondrite-normalized REE profiles of (a) clinopyroxenes; (b) amphiboles; (c) garnets; from the Malaitan spinel- and garnet–spinel-lherzolites. Normalizing data from Nakamura (1974).

described above. This lack of zonation is unlike the amphibole-lherzolites of Nunivak Island, Alaska (Francis, 1976) where spinels mantled by amphibole have increased Cr/(Cr + Al) and decreased Mg/(Mg + Fe) ratios close to the contact with the peridotite mineralogy. The chemical homogeneity displayed by the mineral phases could be due to two processes: (1) extremely rapid equilibration of the major elements within amphibole, spinel and clinopyroxene; and (2) halting of amphibole formation and equilibration of major elements before entrainment in the alnoite and eruption to the surface.

The isotopic disequilibrium between clinopyroxene and amphibole would suggest insufficient time had elapsed for equilibration, and the disparity between isotope ratios and major elements remains a paradox. Isotope results do, however, have four important implications:

(1) The Sr and Nd disequilibrium between clinopyroxene and amphibole suggests that amphibole formed prior to alnoite eruption (model ages suggest $<200$ Ma) and indicates a decoupling of major and trace element equilibration.
(2) The metasomatizing fluid has not originated from the host because of the disparity of $^{87}Sr/^{86}Sr$ ratios between amphiboles and the alnoite (Table 8).

TABLE 9

*REE abundances in lherzolite mineral separates*

| | *La* | *Ce* | *Nd* | *Sm* | *Eu* | *Gd* | *Dy* | *Er* | *Yb* | *Lu* |
|---|---|---|---|---|---|---|---|---|---|---|
| CRN205(SL) | 3·87 | 4·76 | 2·40 | 1·25 | 0·55 | 2·30 | 3·17 | 2·04 | 1·89 | 0·30 |
| CRN216(SL) | 1·52 | 4·33 | 4·71 | 2·08 | 0·86 | 3·09 | 3·76 | 2·10 | 1·87 | 0·27 |
| PHN4009(GSL) | 2·27 | 5·83 | 5·28 | 1·99 | 0·79 | 2·89 | 3·72 | 2·23 | 2·02 | 0·28 |
| PHN4013(GSL) | 10·1 | 41·1 | 22·0 | 2·49 | 0·65 | 1·56 | 0·88 | 0·29 | 0·19 | 0·02 |
| PHN4016(GSL) | 1·02 | 2·75 | 2·91 | 1·26 | 0·52 | 1·92 | 2·31 | 1·58 | 1·22 | 0·17 |
| PHN4064(GSL) | 5·49 | 13·11 | 8·51 | 2·13 | 0·72 | 2·12 | 1·41 | 0·68 | 0·49 | 0·06 |
| PHN4067(GSL) | 2·77 | 7·56 | 6·17 | 1·98 | 0·72 | 2·25 | 1·77 | 0·87 | 0·51 | 0·06 |
| PHN4069(GSL) | 30·7 | 129.0 | 74·3 | 8·96 | 2·55 | 5·96 | 3·47 | 1·09 | 0·51 | 0·04 |
| CRN209(GSL) | 1·22 | 4·26 | 4·30 | 1·36 | 0·48 | 1·48 | 1·02 | 0·35 | 0·20 | 0·02 |
| CRN213(GSL) | 0·61 | 1·75 | 2·51 | 1·28 | 0·55 | 2·12 | 2·79 | 1·64 | 1·42 | 0·20 |
| | | | | *Amphibole* | | | | | | |
| PHN4069(GSL) | 9·46 | 41·5 | 23·1 | 2·71 | 0·69 | 1·66 | 1·34 | 0·28 | 0·14 | 0·01 |
| PHN4074(SL) | 2·57 | 10·9 | 12·7 | 4·27 | 1·59 | 4·42 | 3·24 | 1·18 | 0·71 | 0·07 |
| PHN4085(SL) | 7·03 | 27·1 | 25·1 | 6·84 | 2·36 | 6·73 | 5·14 | 2·33 | 1·40 | — |
| CRN216(SL) | 9·08 | 31·4 | 28·8 | 7·73 | 2·80 | 6·88 | 6·17 | 2·90 | 1·56 | 0·15 |
| | | | | *Garnet* | | | | | | |
| PHN4013(GSL) | 0·90 | 2·71 | 2·72 | 1·27 | 0·64 | 2·43 | 3·09 | 2·25 | 2·61 | 0·51 |
| PHN4064(GSL) | 0·01 | 0·47 | 0·39 | 0·30 | 0·18 | 0·97 | 1·72 | 1·38 | 1·53 | 0·28 |
| PHN4067(GSL) | 0·10 | 0·28 | 0·40 | 0·49 | 0·33 | 1·69 | 4·46 | 3·87 | 4·65 | 0·91 |
| PHN4069(GSL) | 1·09 | 3·10 | 2·99 | 1·36 | 0·69 | 3·75 | 9·00 | 6·45 | 7·06 | 1·13 |
| CRN213(GSL) | 0·05 | 0·15 | 0·16 | 0·26 | 0·25 | 1·55 | 4·09 | 3·45 | 4·25 | 0·72 |

(3) The isotopic and trace element results divide the four analysed amphiboles into three groups: (i) PHN4085 (SL) and CRN216 (SL) ($^{87}Sr/^{86}Sr \cong 0{\cdot}70406$; $\varepsilon Nd \cong +3$; parallel REE patterns, maximum at Nd); (ii) PHN4074 (SL) ($^{87}Sr/^{86}Sr = 0{\cdot}70333$; $\varepsilon Nd = +1{\cdot}2$; convex upwards REE profile, maximum at Sm); and (iii) PHN4069 (GSL) ($^{87}Sr/^{86}Sr = 0{\cdot}70392$; $\varepsilon Nd = +3{\cdot}9$; LREE enriched profile).

(4) The decoupled nature of the enriched Sm/Nd and depleted $^{143}Nd/^{144}Nd$ ratios in the amphiboles indicates recent crystallization and the metasomatic fluid has been derived from a LREE depleted source $< 200$ Ma.

The LREE enrichment reported in clinopyroxenes from six garnet–spinel-peridotites may be due to metasomatism or equilibration of clinopyroxene with garnet. Shimuzu (1975) and Ehrenberg (1982) have measured REE contents of both clinopyroxene and garnet from South Africa and the Colorado Plateau, USA, respectively. In both instances, clinopyroxene and garnet are presumed to be in equilibrium and clinopyroxenes are enriched in the LREE and depleted in HREE. The ability of garnet to accommodate the HREE over the LREE relative to clinopyroxene, results in relative LREE enrichment in clinopyroxene. However, the cause of this LREE enrichment in the Malaitan peridotite clinopyroxenes is defined by the reconstructed whole rock REE profiles (Fig. 7). These demonstrate that LREE enriched clinopyroxenes are from xenoliths with a LREE enriched whole rock pattern. This whole rock LREE enrichment is irreconcilable with garnet–cpx equilibration (although this may have occurred) especially as whole rock Sm/Nd and $^{143}Nd/^{144}Nd$ ratios are decoupled. Therefore, metasomatism in the form of trace element enrichment, is responsible (in part) for the LREE enriched clinopyroxenes. This may or may not be accompanied by modal metasomatism as trace element enrichment is observed in clinopyroxenes from PHN4064 (GSL) and PHN4067 (GSL), xenoliths without any accompanying primary amphibole.

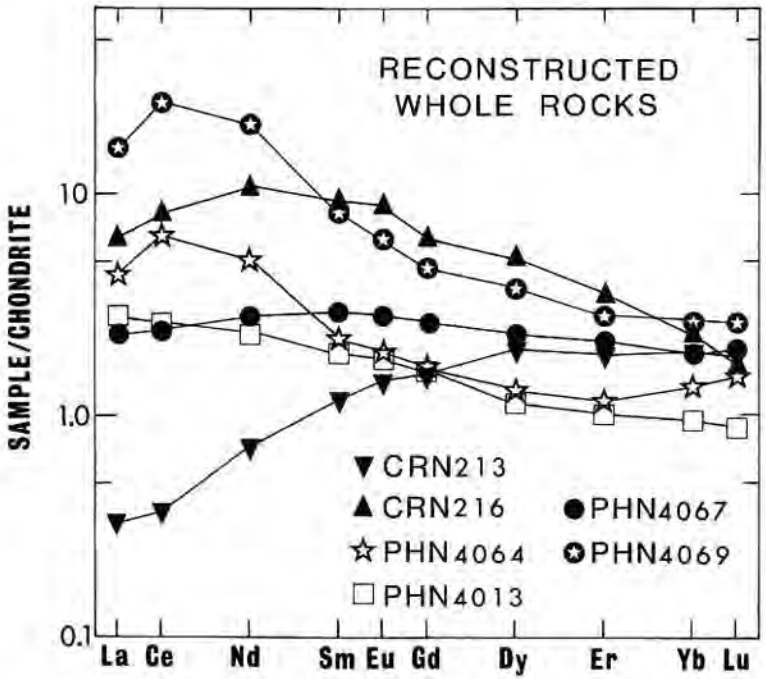


FIG. 7. Reconstructed (chondrite-normalized) whole rock REE profiles using measured mineral REE compositions and estimated modal proportions. The LREE enriched nature of all but CRN213 and PHN4067 indicates metasomatism by trace element enrichment. All have $^{143}Nd/^{144}Nd$ ratios > bulk earth. PHN4067 has a flat REE profile, but a $^{143}Nd/^{144}Nd$ ratio > bulk earth, suggesting this xenolith has also experience some degree of trace element enrichment. All samples except CRN213, have decoupled Sm/Nd and $^{143}Nd/^{144}Nd$ ratios.

Clinopyroxenes from seven of the eight garnet–spinel-lherzolites show a positive correlation between the Sm/Nd and $^{143}Nd/^{144}Nd$ ratios yielding an apparent isochron age of 240 $\pm$10 Ma (Fig. 8). CRN209 (GSL) has not been included in this study because it is petrographically (kelyphitized garnets) and chemically dissimilar to the other garnet–spinel-lherzolites. The significance of this apparent age is important to determine.

Zindler *et al.* (1984) have undertaken Sr and Nd isotope studies on young Pacific seamounts, and have noted isochronus relationships between these with both Rb–Sr and Sm–Nd results yielding comparable ages of 230 and 260 Ma, respectively. A linear relationship of positive slope on a diagram of the form $^{87}Sr/^{86}Sr$ vs. $^{87}Rb/^{86}Sr$ or $^{143}Nd/^{144}Nd$ vs. $^{147}Sm/^{144}Nd$ reflects either the preservation of an 'isochron' or the occurrence of some two component mixing process (e.g., Langmuir *et al.*, 1978). Zindler *et al.* (1984) postulate two component mixing lines instead of isochron ages for their correlations, suggesting heterogeneities within the mantle have existed for at least as long as indicated by the isochron age. It is considered that the Malaitan data also represents a mixing line and the following discussion outlines the evidence for such a supposition.

### *Evidence for two component mixing*

Hawkesworth & Vollmer (1979) have shown two component mixing is evident from an isochronus relationship for both Rb–Sr and Sm–Nd data from Roccamonfina, Italy. In

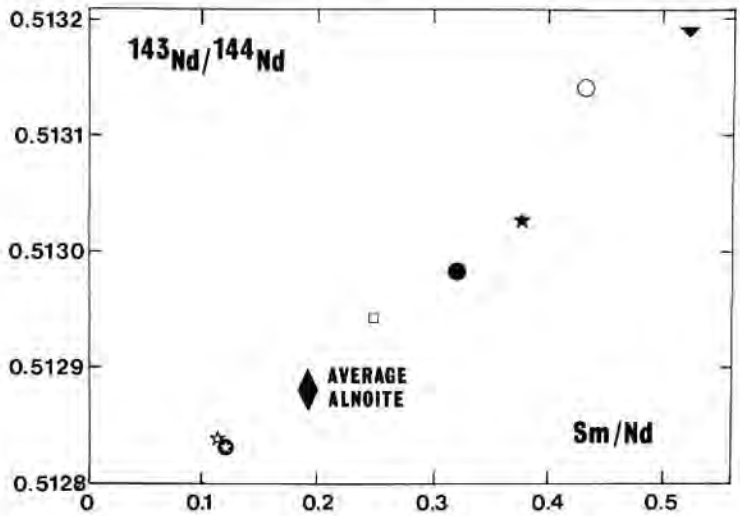


FIG. 8. $^{143}Nd/^{144}Nd$ vs. Sm/Nd of clinopyroxenes from 7 garnet–spinel-lherzolites. The age represented is 240 ± 10 Ma. Also plotting in the centre of this correlation is the host alnoite (diamond).

addition they demonstrate that two component mixing results in a linear relationship of positive slope on a diagram of $^{143}Nd/^{144}Nd$ vs. 1/Nd. Figure 9a shows such a relationship for the Malaitan clinopyroxenes and the good fit of a straight line through the data is a measure of when the mixing occurred, in that if mixing is ancient, subsequent radioactive decay is likely to scatter the data (Hawkesworth & Vollmer, 1979). The lack of any major scatter on the Sm–Nd isochron plot (Fig. 8) suggests a relatively recent mixing event, which is supported by the decoupled nature of the Nd isotopes in samples displaying LREE enrichment.

No linear relationship is seen for $^{87}Sr/^{86}Sr$ vs. 1/Sr (Fig. 9b) indicating that either two component mixing has not affected Rb–Sr in these samples, or has been masked by a later process affecting Rb–Sr only. PHN4069, PHN4013, PHN4064, and PHN4067 form a negative correlation, but PHN4009, PHN4016, and CRN213 plot to the right. Clinopyroxenes from PHN4009, PHN4016, and CRN213 have Sr and Nd isotopes similar to the spinel-lherzolites, as are the REE patterns which all have a slight enrichment at La (exemplified by CRN205 (SL) and the rest of the spinel-lherzolites; Neal, 1985). It is considered that these three xenoliths have experienced another metasomatic enrichment, in Sr only, similar to that exhibited by the spinel-lherzolites (Neal, 1985). As the $^{87}Sr/^{86}Sr$ results have been duplicated after stringent leaching, the lack of correlation in Fig. 9b is not a function of surface contamination. Hence the use of Rb–Sr results to calculate model ages for either of these events will be impossible, but Sm–Nd model ages from clinopyroxenes may be used to identify the approximate age of mixing. CRN213 falls at the upper end of the mixing line (Fig. 8). This sample represents a MORB source and the depletion age of 612 Ma $T_{BE}$ (Fig. 10) will represent the maximum age of the final depletion this xenolith has experienced. PHN4013 falls at the opposite end of the mixing line to CRN213 and gives the youngest calculated enrichment age of 528 Ma $T_{MORB}$ (Fig. 10). This is taken as the maximum age for the metasomatic event as PHN4013 lies at the opposite end of the mixing line to CRN213 (Fig. 8). All other ages are of no significance as they represent mixes between a MORB source (represented by CRN213) and the metasomatic fluid. Meta-

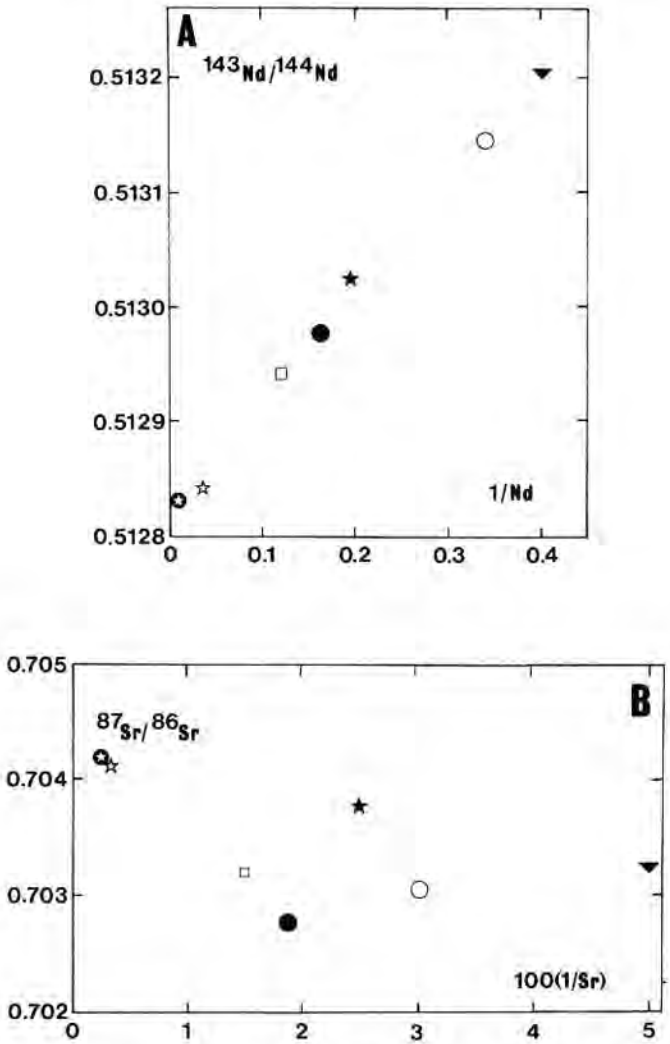


FIG. 9. (a) $^{143}Nd/^{144}Nd$ vs. 1/Nd of clinopyroxenes in Fig. 8; (b) $^{87}Sr/^{86}Sr$ vs. 100(1/Sr) for clinopyroxenes in Fig. 8. Symbols as in Fig. 6. Isotope data are corrected to the age of eruption (34 Ma, Davis, 1977).

somatism can be considered to 'rotate' the evolution line of CRN213 to that of PHN4013 (Fig. 10). Therefore, the point at which the evolution lines cross will give an approximate age for the mixing or metasomatic event (240 Ma). The age is the same as that given by the 'pseudoisochron', suggesting this may also be representative of the age of mixing.

PHN4013 and PHN4069 have been most affected by the metasomatic fluid responsible for the mixing line in Fig. 8. They have not only the highest Sr abundances (272 and 400 p.p.m. respectively), but also the most radiogenic $^{87}Sr/^{86}Sr$ ratios (0·703931 and 0·704047 respectively). The clinopyroxene and garnet REE patterns of these two xenoliths are similar to each other (see section 5). Clinopyroxenes in both of these samples have been involved in garnet growth (Neal & Nixon, 1986) whereas clinopyroxenes in other xenoliths

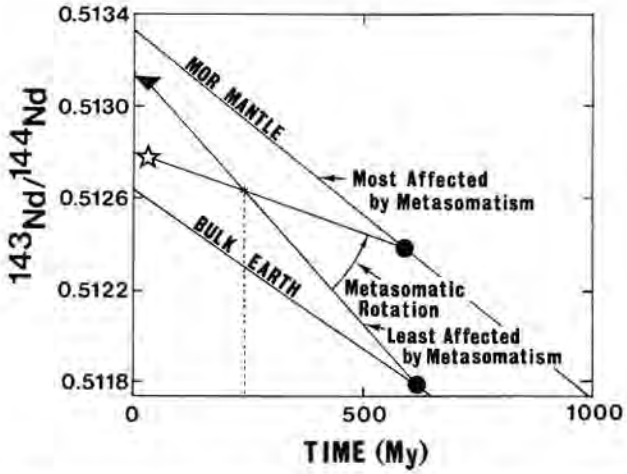


FIG. 10. Nd model ages calculated from $PHN4013_{cpx}$ (representing the metasomatic fluid) and $CRN213_{cpx}$ (representing a MORB mantle source). These two xenoliths form end-members on the Sm–Nd mixing line (Fig. 8). The variable LREE enrichment of the suite of garnet–spinel-lherzolites results in the 'rotation' of the evolution line calculated for CRN213. This rotation eventually results in the evolution line calculated for PHN4013. The cross over point indicates the age of mixing. The MOR mantle evolution line is taken from Zindler & Jagoutz (1986). Symbols as in Fig. 6.

have not. Other xenoliths of similar mineralogy contain clinopyroxenes which are generally more enriched in HREE and less in LREE. In PHN4009, PHN4016, PHN4064, PHN4067, and CRN213, garnet has formed by the reaction of amphibole and spinel (Neal, 1985; Neal & Nixon, 1986). Sr disequilibrium between clinopyroxene and garnet in PHN4064 and PHN4067 can be explained by contamination from the host alnoite (Fig. 11). However, it can be argued that the garnets have inherited the isotopic signature from amphibole because:

(1) of the four garnets analysed for Sr, the two in isotopic equilibrium with clinopyroxenes have formed from clinopyroxene + spinel (PHN4013 and PHN4069), and those in Sr isotopic disequilibrium have formed from amphibole + spinel (PHN4064 and PHN4067). Selective contamination of two out of four analysed seems somewhat fortuitous, as the same leaching procedures have been carried out on all mineral separates.

(2) REE contents of clinopyroxenes from xenoliths where garnet has formed from spinel + amphibole (PHN4064 and PHN4067) have generally higher HREE abundances indicating lack of equilibration with garnet.

(3) REE contents of garnets formed from clinopyroxene + spinel (PHN4013 and PHN4069) display a flattening of the LREE to $La_N \cong 3$ and where garnet has formed from spinel + amphibole, $La_N < 1$.

(4) Rb–Sr isochron ages calculated from mineral separates of PHN4064 and PHN4067 are spurious as widely differing ages result. Sm–Nd results form a negative correlation on a $^{143}Nd/^{144}Nd$ vs. $^{147}Sm/^{144}Nd$ diagram, such as noted by Richardson *et al.* (1982, 1985) and Basu & Tatsumoto (1979, 1980). Richardson *et al.* (1982, 1985) consider this to be the result of metasomatic addition without re-equilibration.

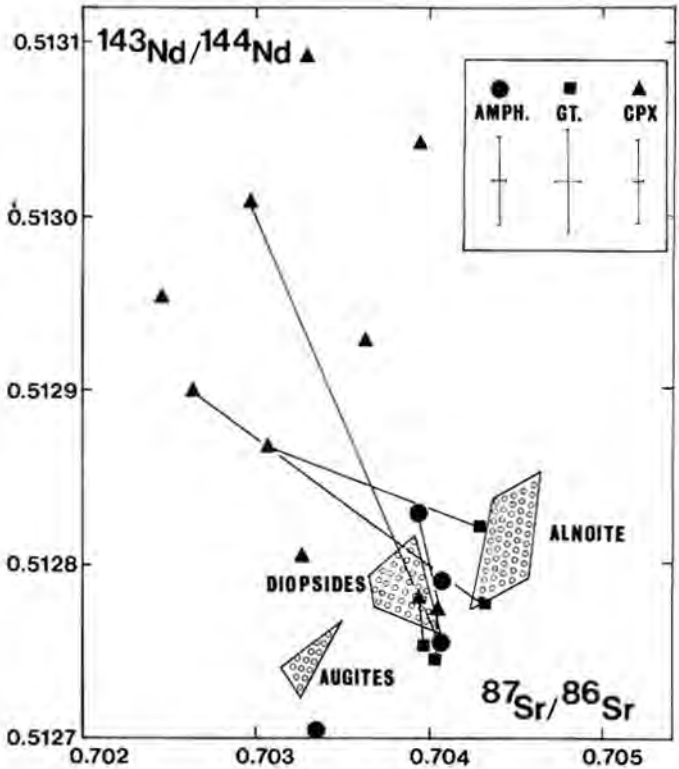


FIG. 11. $^{143}Nd/^{144}Nd$ vs. $^{87}Sr/^{86}Sr$ diagram of all data collected. Tie lines indicate co-existing phase. The fields of augite and subcalcic diopside megacrysts, and the host alnoite are represented. The analysed amphiboles are isotopically similar to the megacryst fields rather than the host alnoite. All data are corrected to the age of alnoite eruption.

### *Origin of the metasomatic fluid*

Textural evidence of metasomatism in mantle xenoliths demonstrates that two component mixing can be envisaged as a result of fluid migration (Erlank, 1976). The most plausible 'fluid' which may have been involved in any metasomatic event beneath the Solomon Islands is the host alnoite. Significantly, if the isochron plot is re-examined (Fig. 8), the alnoite host lies towards the centre of the array, between PHN4069 and PHN4064. This observation, coupled with the isotopic disparity between amphiboles and the alnoite, indicates trace element enrichment and modal metasomatism were not related to the host alnoite.

The REE patterns of the metasomatic fluid can be estimated from the REE profiles of the amphiboles analysed, using amphibole/liquid partition co-efficients of Higuchi & Nagasawa (1969), and Irving & Price (1981). These results (Table 10) indicate that three types of fluid may have been responsible for the crystallization of amphibole (reflecting the amphibole REE), or one evolving fluid depositing amphibole over a period of time. None of these calculated 'equilibrium liquids' resembles the host alnoite.

Neal (1988) presents a model which the alnoite and megacryst suite are inferred to have developed from a mantle diapir which impinged upon the rigid lithosphere and crystallized

TABLE 10

*Calculated equilibrium liquids for amphiboles and clinopyroxene megacrysts, compared with alnoite and alkali basalt*

| *Kd Reference* | | *La/Yb* | *Ce/Yb* |
|---|---|---|---|
| | Alkali Basalt | 17·4 | 36·1 |
| | Alnoite | 45–55 | 88–99 |
| Grutzeck *et al.* (1974) | | | |
| | Diopsides | 17·3–25·5 | 42·8–57·7 |
| | Augites | 15·3–17·7 | 44·9–47·9 |
| Higuchi & Nagasawa (1969) | | | |
| | PHN4074 | 21·4 | 44·9 |
| | PHN4085 | 29·4 | 55·9 |
| | CRN216 | 34·2 | 58·4 |
| | PHN4069 | 404 | 877 |
| Schnetzler & Philpotts (1970) | | | |
| | Diopsides | — | 34·7–48·8 |
| | Augites | | 33·5–39·8 |
| Irving & Price (1981) | | | |
| | PHN4074 | 15·3 | 36·3 |
| | PHN4085 | 20·1 | 43·3 |
| | CRN216 | 24·0 | 46·5 |
| | PHN4069 | 282 | 692 |

the megacryst suite. A subducted derivative of seawater altered basalt is inferred to underplate the lithosphere in this region (see Hussong *et al.*, 1979). From isotopic evidence, it was inferred that the augite megacrysts crystallized first and the subcalcic diopsides concluded clinopyroxene megacryst fractionation. Calculated equilibrium liquids from $PHN4074_{amphibole}$ resemble those from the augite megacrysts, whereas those from $CRN216_{amphibole}$ and $PHN4085_{amphibole}$ resemble those from the subcalcic diopside megacrysts (Table 10). It is concluded that amphibole in PHN4074(SL) crystallized from fluids emanating from the mantle diapir ('*proto-alnoite*') shortly after impingement (during the beginning of augite crystallization). Amphibole in PHN4085(SL) and CRN216(SL) crystallized later from fluids emanating from the proto-alnoite during subcalcic diopside megacryst crystallization. PHN4069(GSL) contains amphibole with a REE pattern which is similar to that of the clinopyroxene. The equilibrium liquid calculated from the amphibole has a steep REE pattern (La/Yb = 282) which cannot be related to any feasible calculated equilibrium liquid. It is considered that the LREE enriched signature of the clinopyroxene in PHN4069(GSL), has been inherited by the amphibole (see earlier). However, the resulting Sm/Nd ratio has had insufficient time to alter the $^{143}Nd/^{144}Nd$ ratio inherited by $PHN4069_{amphibole}$ from the metasomatic fluid. In other xenoliths clinopyroxene contains low LREE abundances (e.g., CRN216(SL)) thus having little effect upon the REE content of amphibole.

Isotope results support the conclusions of REE modelling (Fig. 11). $PHN4074_{amphibole}$ is within error of the augite megacryst range, and $PHN4069_{amphibole}$, $PHN4085_{amphibole}$, and $CRN216_{amphibole}$ are within error of the subcalcic diopside megacryst range for both Sr and Nd isotopes. It appears that $PHN4069_{amphibole}$ was precipitated during the crystallization of the subcalcic diopside megacrysts on the basis of these isotope data. The Sr and Nd results from $PHN4069_{cpx}$ and $PHN4013_{cpx}$ are isotopically within error of the subcalcic diopside megacrysts. As these lie at one end of the mixing line (Fig. 8), this would suggest that the mixing line was also generated at this time.

From Fig. 11 $^{87}Sr/^{86}Sr$ and $^{143}Nd/^{144}Nd$ become more radiogenic with progressive megacryst fractionation due to the assimilation of seawater-altered basalt (Neal, 1988). This scenario requires the proto-alnoite to evolve by an assimilation and fractional crystallization process with the continual emanation of hydrous fluids into the surrounding mantle. These fluids would have the isotopic and trace element characteristics of the proto-alnoite, which would vary according to the evolution of the proto-alnoite. As a result, such metasomatism is a consequence of, not a prerequisite for alnoite magmatism.

## CONCLUSIONS

Garnet- and spinel-bearing xenoliths from the Malaitan alnoite have been metasomatized by a $H_2O$-rich fluid containing $CO_2$, Na, K, Fe, Sr, Rb, Ti, and REE, resulting in both trace element enrichment and modal metasomatism. These fluids were derived from a molten mantle diapir or 'proto-alnoite' which impinged on the base of the rigid lithosphere, crystallizing the megacryst suite. As megacryst fractionation progressed (augite→subcalcic diopside), the proto-alnoite developed a steeper REE profile and also assimilated a subducted MORB derivative that underplates the Ontong Java Plateau. Assimilation of this component manifests itself in progressively more radiogenic Sr and Nd isotope ratios in later fractionated megacrysts (the subcalcic diopsides). During megacryst fractionation, $H_2O$-rich fluids continually emanated into the surrounding mantle from the molten diapir. Amphiboles crystallized from reaction of this fluid with anhydrous peridotite resulted in amphibole crystallization. These amphiboles record the evolution of the proto-alnoite as it underwent assimilation and fractional crystallization, resulting ultimately in the development of the alnoite host that is seen at the surface today.

## ACKNOWLEDGEMENTS

Many thanks go to Peter Nixon, Gareth Davies, and Jon Davidson for valuable discussions and criticisms. A special thank you is extended to the Government of the Solomon Islands and the people of northern Malaita (especially Chief Selwyn Wandilli). Their help and hospitality made the field work possible and my stay in their country enjoyable. Professor Larry Taylor of the University of Tennessee is acknowledged for his valuable contributions (both financial and scientific). The staff of the Isotope Laboratory at Leeds University showed great patience during my time there and are also thanked. I am greatly indebted to Eric Condliffe for guidance in the use of the Electron Microprobe. This study was funded by a grant from the Natural Environment Research Council.

## REFERENCES

Bailey, D. K., 1982. Mantle metasomatism—continuing change within the earth. *Nature*, **296**, 525–30.

Basu, A. R., & Tatsumoto, M., 1979. Sm–Nd systematics in kimberlites and in the minerals of garnet lherzolite inclusions. *Science*, **205**, 398–401.

——— 1980. Nd isotopes in selected mantle-derived rocks and minerals and their implications for mantle evolution. *Contr. Miner. Petrol.* **75**, 43–54.

Bergman, S. C., Foland, K. A., & Spera, F. J., 1981. On the origin of an amphibole-rich vein in a peridotite inclusion from Lunar Crater Volcanic Field, Nevada, U.S.A. *Earth Planet. Sci. Lett.* **56**, 343–61.

Best, M. G., 1970. Kaersutite-peridotite inclusion and kindred megacrysts in basanitic lavas, Grand Canyon, Arizona. *Contr. Miner. Petrol.* **27**, 25–44.

——— 1974. Mantle-derived amphibole within inclusions in alkali-basaltic lavas. *J. Geophys. Res.* **79**, 2107–13.

——— 1975. Amphibole-bearing cumulate inclusions in basanite, Grand Canyon, Arizona and their bearing on silica undersaturated hydrous magmas in the upper mantle. *J. Petrology* **16**, 212–36.

Boettcher, A. L., O'Neill, J. R., Windom, J. E., Stewart, D. C., & Wilshire, H. G., 1979. Metasomatism of the upper mantle and genesis of kimberlite and other volcanics. In: Boyd, F. R., & Meyer, H. O. A. (eds) *Kimberlites, Diatremes and Diamonds*. Washington: AGU, 173–82.

Boyd, F. R., 1971. Pargasite–spinel peridotite xenolith from the Wesselton Mine. *Yb. Carnegie Inst. Wash.* **70,** 138–42.

Clague, D. A., & Frey, F. A., 1982. Petrology and trace element geochemistry of the Honolulu Volcanics, Oahu: implications for the oceanic mantle below Hawaii. *J. Petrology* **23,** 447–504.

Conquere, F., 1971. La lherzolite a amphibole du gisment de Causson (Ariege, France). *Contr. Miner. Petrol.* **30,** 296–313.

Davis, G. L., 1977. The ages and uranium contents of zircons from kimberlites and associated rocks. Extended abstracts, *2nd International Kimberlite Conf.* Arizona.

Dawson, J. B., 1984. Contrasting types of upper mantle metasomatism? In: Kornprobst, J. (ed.) *Kimberlites II: Crust and Crust–Mantle Relationships*. Elsevier, 289–94.

—— Smith, J. V., 1982. Upper mantle amphiboles: a review. *Miner. Mag.* **45,** 35–46.

Deer, W. A., Howie, R. A., & Zussman, J., 1978. *An Introduction to the Rock-Forming Minerals* (eleventh impression). Longman, 527 pp.

Ehrenberg, S. N., 1982. REE geochemistry of garnet lherzolite and megacrystalline nodules from minette of the Colorado Plateau Province. *Earth Planet. Sci. Lett.* **57,** 191–210.

Erlank, A. J. 1976. Upper mantle metasomatism as revealed by potassic richterite-bearing peridotite xenoliths from kimberlites. *EOS* **57,** 597.

Francis, D. M., 1976. The origin of amphibole in lherzolite xenoliths from Nunivak Island, Alaska. *J. Petrology* **17,** 357–78.

—— 1978. The implications of the compositional dependence of texture in spinel lherzolite xenoliths. *J. Geol.* **86,** 473–85.

Frey, F. A., Green, D. H., & Roy, S., 1978. Integrated models of basalt petrogenesis: a study of quartz tholeiites to olivine melilitites from southeastern Australia utilizing geochemical and experimental petrological data. *J. Petrology* **19,** 463–513.

Green, D. H., 1973. Experimental melting studies on model upper mantle compositions at high pressures under both water-saturated and water-undersaturated conditions. *Earth Planet. Sci. Lett.* **19,** 37–53.

Grutzeck, M., Kridelbaugh, S., & Weill, D., 1974. The distribution of Sr and REE between diopside & silicate liquid. *Geophys. Res. Lett.* **1,** 273–75.

Harte, B., 1977. Rock nomenclature with particular relation to deformation and recrystallization textures in olivine-bearing xenoliths. *J. Geol.* **85,** 279–88.

—— 1983. Mantle peridotites and processes, the kimberlite sample. In: Hawkesworth, C. J., & Norry, M. J. (eds) *Continental Volcanics and Mantle Xenoliths*, 46–91.

Hawkesworth, C. J., & Vollmer, R., 1979. Crustal contamination versus enriched mantle: $^{143}Nd/^{144}Nd$ and $^{87}Sr/^{86}Sr$ evidence from the Italian volcanics. *Contr. Miner. Petrol.* **69,** 151–65.

Higuchi, H., & Nagasawa, H., 1969. Partition of trace elements between rock-forming minerals and the host volcanic rocks. *Earth Planet. Sci. Lett.* **7,** 281–7.

Hussong, D. M., Wipperman, L. K., & Kroenke, L. W., 1979. The crustal structure of the Ontong Java and Manihiki ocean Plateaus. *J. Geophys. Res.* **84,** 6003–10.

Irving, A. J., & Price, R. C., 1981. Geochemistry and evolution of lherzolite-bearing phonolite lavas from Nigeria, Australia, East Germany and New Zealand. *Geochim. Cosmochim. Acta* **45,** 1309–20.

Kay, R. W., & Gast, P. W., 1973. The rare earth content of alkali-rich basalts. *J. Geol.* **81,** 653–82.

Langmuir, C. H., Vocke, R. D., & Hanson, G. N., 1978. A general mixing equation with application to Icelandic basalts. *Earth Planet. Sci. Lett.* **37,** 380–92.

Leake, B. E., 1978. Nomenclature of amphiboles. *Am. Miner.* **63,** 1023–52.

Lindsley, D. H., & Andersen, D. J., 1983. A Two-Pyroxene Thermometer. *J. Geophys. Res.* **88,** A887–906.

Menzies, M. A., Kempton, P., & Dungan, M., 1985. Interaction of continental lithosphere and asthenospheric melts below the Geronimo Volcanic Field, Arizona, U.S.A. *J. Petrology* **26,** 663–93.

Leeman, W. P., & Hawkesworth, C. J., 1983. Isotope geochemistry of Cenozoic volcanic rocks reveals mantle heterogeneity below western U.S.A. *Nature* **303,** 205–09.

—— Hawkesworth, C. J., (eds.) 1987. *Mantle Metasomatism*. London: Academic Press, 477 pp.

—— Murthy, V. R., 1980*a*. Nd and Sr isotope geochemistry of hydrous mantle nodules and their host alkali basalts: implications for local heterogeneities in metasomatically veined mantle. *Earth Planet. Sci. Lett.* **46,** 323–34.

—— —— 1980*b*. Mantle metasomatism as a precursor to the genesis of alkaline magmas—isotopic evidence. *Am. J. Sci.* **280A,** 622–38.

—— Wass, S. Y., 1983. $CO_2$-rich mantle below eastern Australia: REE, Sr and Nd isotopic study of Cenozoic alkaline magmas and apatite-bearing xenoliths from the Southern Highlands Province, New South Wales, Australia. *Earth Planet. Sci. Lett.* **65,** 287–302.

Nakamura, N., 1974. Determination of REE, Ba, Fe, Mg, Na, and K in carbonaceous and ordinary chondrites. *Geochim. Cosmochim. Acta* **38,** 757–76.

Neal, C. R., 1985. Mantle Studies in the Western Pacific and Kimberlite-type intrusives. Unpub. Ph.D. Thesis, Univ. Leeds, England.

——1988. An unmetasomatized source for the Malaitan alnoite: Petrogenesis involving zone refining, megacryst fractionation, and crustal assimilation. *Geochim. Cosmochim. Acta* (in press).
——Nixon, P. H., 1986. Spinel–garnet relationships in mantle xenoliths from the Malaita alnoite, Solomon Islands, South-Western Pacific. *Trans. Geol. Soc. South Africa* **88,** 347–54.
Nixon, P. H., Rogers, N. W., Gibson, I. L., & Grey, A., 1981. Depleted and fertile xenoliths from Southern African kimberlites. *Ann. Rev. Earth Planet. Sci.* **9,** 285–309.
O'Hara, M. J., Saunders, M., & Mercy, P. L., 1975. Garnet periodotite, possible ultrabasic magmas and eclogite; interpretation of upper mantle processes in kimberlite. *Phys. Chem. Earth* **9,** 681–713.
Richardson, S. H., Erlank, A. J., & Hart, S. R., 1985. Kimberlite-borne peridotite xenoliths from old enriched subcontinental lithosphere. *Earth Planet. Sci. Lett.* **75,** 116–28.
——Shimuzu, N., 1982. Nd isotopic disequilibrium in garnet peridotites from the Bultfontein kimberlite, and implications for mantle metasomatic component addition. *Terra Cognita* **2,** 231–32.
Roden, M. F., Frey, F. A., & Francis, D. M., 1983. An example of consequent metasomatism in peridotite inclusions from Nunivak Island, Alaska. *J. Petrology* **25,** 546–77.
Schnetzler, C. C., & Philpotts, J. A., 1970. Partition coefficients of REE between igneous matrix material and rock-forming phenocrysts-II. *Geochim. Cosmochim. Acta* **34,** 331–40.
Shimuzu, N., 1975. REE in garnet and clinopyroxene from garnet lherzolite nodules in kimberlite. *Earth Planet. Sci. Lett.* **25,** 26–32.
Stosch, H. G., & Seck, H. A., 1980. Geochemistry and mineralogy of two spinel peridotite suits from Dreiser Weiher, West Germany. *Geochim. Cosmochim. Acta* **44,** 457–70.
Sun, S., & Hanson, G. N., 1975. Origin of Ross Island basanitoid and limitations upon the heterogeneity of mantle sources for alkali basalts and nephelinites. *Contr. Miner. Petrol.* **52,** 77–106.
Varne, R., 1970. Hornblende lherzolite and the upper mantle. *Ibid.* **27,** 45–51.
——Graham, A. L., 1971. Rare earth abundance in hornblende and clinopyroxene of a hornblende lherzolite xenolith. Implications for upper mantle fractionation processes. *Earth Planet. Sci. Lett.* **13,** 11–8.
Wass, S. Y., & Rogers, N. W., 1980. Mantle metasomatism—precursor to continental alkaline volcanism. *Geochim. Cosmochim. Acta.* **44,** 1811–23.
Wilshire, H. G., Pike, J. E. N., Meyer, C. E., & Schwarzmann, E. C., 1980. Amphibole-rich veins in lherzolite xenoliths, Dish Hill, California. *Am. Miner.* **56,** 240–55.
Wyllie, P. J., 1977. Mantle fluid compositions buffered by carbonates in peridotite–$CO_2$–$H_2O$. *J. Geol.* **85,** 187–207.
——1978. Mantle fluid compositions buffered in peridotite–$CO_2$–$H_2O$ by carbonates, amphibole and phlogopite. *Ibid.* **86,** 687–713.
——1980. The origin of kimberlite. *J. Geophys. Res.* **85,** 6902–10.
Zindler, A., & Jagoutz, E., 1980. Isotope and trace element systematics in mantle-derived peridotite nodules from San Carlos. *EOS* **61,** 374.
——1986. Trace elements and Nd and Sr isotope systematics of peridotite nodules from Pridot Mesa, San Carlos, Arizona. *Geochim. Cosmochim. Acta* (in press).
——Staudigel, H., & Batiza, R., 1984. Isotope and trace element geochemistry of young Pacific seamounts: implications for the scale of upper mantle heterogeneity. *Earth Planet. Sci. Lett.* **70,** 175–95.